

# Variable tree rooting strategies are key to model distribution, productivity and evapotranspiration of tropical evergreen forests

Boris Sakschewski<sup>1</sup>, Werner von Bloh<sup>1</sup>, Markus Drüke<sup>1,2</sup>, Anna Amelia Sörensson<sup>3,4</sup>, Romina Ruscica<sup>3,4</sup>, Fanny Langerwisch<sup>5,6</sup>, Maik Billing<sup>1</sup>, Sarah Bereswill<sup>7</sup>, Marina Hirota<sup>8,9</sup>, Rafael Silva Oliveira<sup>9</sup>, Jens Heinke<sup>1</sup>, Kirsten Thonicke<sup>1</sup>

<sup>1</sup>Potsdam Institute for Climate Impact Research, Potsdam, 14473, Germany

<sup>2</sup>Humboldt Universität zu Berlin, Unter den Linden 6, 10099 Berlin, Germany

<sup>3</sup>Universidad de Buenos Aires - Consejo Nacional de Investigaciones Científicas y Técnicas, Centro de Investigaciones del Mar y la Atmósfera (CIMA/UBA-CONICET), Buenos Aires, Argentina.

<sup>4</sup>Institut Franco-Argentin d'Etudes sur le Climat et ses Impacts, Unité Mixte Internationale (UMI-IFAECI/CNRS-CONICET-UBA), Argentina

<sup>5</sup>Czech University of Life Sciences Prague, Department of Water Resources and Environmental Modeling, 165 00 Praha 6 – Suchbátka, Czech Republic

<sup>6</sup>Palacký University Olomouc, Department of Ecology and Environmental Sciences, 78371 Olomouc, Czech Republic

<sup>7</sup>University of Potsdam, Potsdam, 14469, Germany

<sup>8</sup>Federal University of Santa Catarina (UFSC), Campus Universitário Reitor João David Ferreira Lima Trindade – Florianópolis – SC, CEP: 88040-900, Santa Catarina, Brazil

<sup>9</sup>University of Campinas (UNICAMP) Cidade Universitária "Zeferino Vaz" CEP 13083-970, Campinas-SP, Sao Paulo, Brazil

Correspondence to: Boris Sakschewski ([boris.sakschewski@pik-potsdam.de](mailto:boris.sakschewski@pik-potsdam.de))

**Abstract.** A variety of modelling studies have suggested tree rooting depth as a key variable to explain evapotranspiration rates, productivity and the geographical distribution of evergreen forests in tropical South America. However, none of those studies acknowledged resource investment, timing and physical constraints of tree rooting depth within a competitive environment, undermining the ecological realism of their results. Here, we present an approach of implementing variable rooting strategies and dynamic root growth into the LPJmL4.0 DGVM and apply it to tropical and sub-tropical South-America under contemporary climate conditions. We show how competing rooting strategies which underlie the trade-off between above- and below-ground carbon investment lead to more realistically simulation of intra-annual productivity and evapotranspiration, and consequently simulated forest cover and spatial biomass distribution. We find that climate and soil depth determine a spatially heterogeneous pattern of mean rooting depth and belowground biomass across the study region. Our findings support the hypothesis that the ability of evergreen trees to adjust their rooting systems to seasonally dry climates is crucial to explain the current dominance, productivity and evapotranspiration of evergreen forests in tropical South America.

## 1 Introduction

Tropical evergreen forest is the naturally dominant biome type in South-America over a large climatic range including regions with a marked dry season (Hirota et al., 2011; Xiao et al., 2006). To withstand seasonal shortages of precipitation and sustain productivity, trees with evergreen phenology often have access to deep soil water via deep roots (Brum et al., 2019; Canadell et al., 1996; Johnson et al., 2018; Kim et al., 2012; Markewitz et al., 2010). Consequently, recent studies suggest a heterogeneous spatial pattern of maximum rooting depth across tropical forest biomes in South-America which differs over the order of magnitudes depending on local groundwater, soil and climate conditions (Canadell et al., 1996; Fan et al., 2017). So far different modelling approaches were presented which highlighted the crucial role of rooting depth for the productivity and therefore the distribution of evergreen trees in South-America. In a pioneering study more than 20 years ago, Kleidon and Heimann (1998) systematically searched for rooting strategies which yield highest net primary productivity over South America with a dynamic global vegetation model (DGVM) to explain intra-annual rates of ET and vegetation cover. Follow up studies further underlined the importance of deep roots for the water cycle of South America (Kleidon and Heimann, 2000). Accordingly, Lee *et al.* (2005) found that allowing for deep roots and hydraulic redistribution of water in

47 the soil column in a general circulation model (GCM) improved simulated Amazon forest productivity and  
48 evapotranspiration (ET) in the dry season. Baker *et al.* (2008) came to similar results when introducing deep roots in a land  
49 surface model. Ichii *et al.*, (2007) found that constraining rooting depth across the Amazon based on satellite-derived data of  
50 forest productivity yields similar results in a terrestrial ecosystem model. More recently, Langan, Higgins and Scheiter  
51 (2017) showed for the same study area how diverse rooting strategies in a tree individual and trait-based DGVM can  
52 improve simulated intra-annual productivity and ET as well as better explain patterns of different tropical biome types and  
53 biomass in fire-prone ecosystems. While these studies are important steps to acknowledge the diversity of tree rooting depth  
54 and its effects on ET and forest productivity, some assumptions of the underlying models might decrease the liability of their  
55 results. These assumptions are related to 1) resource investment, 2) temporal growth and 3) physical constraints of rooting  
56 depth:

57 1) Most global vegetation models so far do not account for coarse roots (Warren *et al.*, 2015a) even though they can make  
58 up the majority of total root biomass (Xiao *et al.*, 2003). This approach may be sufficient when employing shallow tree  
59 rooting strategies only, but with increasing rooting depth, costs for coarse roots increases substantially. Since the amount of  
60 resources trees can allocate to their processes and structures is finite, a local adaptation of tree rooting depth must follow a  
61 trade-off between above- and below-ground resource investment (Nikolova *et al.*, 2011). Generally, above-ground  
62 investments into leaf and stem growth can increase light absorption and CO<sub>2</sub> uptake, while below-ground investments can  
63 increase the uptake of water and nutrients. Depending on local environmental and competitive conditions one or the other  
64 allocation strategy might be more advantageous, eventually leading to substantial regional variation in the mean ratios  
65 between below-ground to above-ground biomass (Leuschner *et al.*, 2007; Mokany *et al.*, 2006). Therefore, the simulated  
66 spectrum of tree rooting strategies which can survive and co-exist should be in accordance with this crucial trade-off. 2) In  
67 contrast to above-ground stem growth, most global vegetation models do not simulate gradual root growth (Warren *et al.*,  
68 2015a). Instead simulated vegetation types are assigned a constant relative distribution of fine roots throughout the soil  
69 column at any point in space and time (Best *et al.*, 2011; Lawrence *et al.*, 2011; Schaphoff *et al.*, 2018a; Smith *et al.*, 2014).  
70 As under the above-mentioned simplification under 1), this approach may be sufficient when accounting for shallow rooting  
71 strategies only, but when the maximum tree rooting depth is strongly increased, it is questionable that the time needed to  
72 reach this depth is negligible, especially when accounting for competition of different vegetation types. Rooting depth  
73 increases rather gradually and non-linearly over a tree's lifetime with a velocity driven by a mix of plastic optimization and  
74 allometric determination (Brum *et al.*, 2019; Brunner *et al.*, 2015; Nikolova *et al.*, 2011; Poorter *et al.*, 2012; Warren *et al.*,  
75 2015b). Even though smaller-scale models have implemented root optimization schemes in the past (Schymanski *et al.*,  
76 2008), the knowledge base for a mechanistic bottom-up modelling approach of plastic root optimization is very sparse  
77 (Jenik, 2010; Poorter *et al.*, 2012; Warren *et al.*, 2015b) and knowledge on certain allometric rules (Brum *et al.*, 2019; Eshel  
78 and Grünzweig, 2013; Mokany *et al.*, 2006) seems enough to be applied in global vegetation models. 3) Most global  
79 vegetation models so far do not account for a location-dependent soil depth, but apply a constant soil depth across the globe  
80 (Best *et al.*, 2011; Guimberteau *et al.*, 2017; Lawrence *et al.*, 2011; Ostle *et al.*, 2009; Schaphoff *et al.*, 2018a; Smith *et al.*,  
81 2014). Again, this approach may be sufficient when accounting for shallow rooting strategies only, but allowing for deep  
82 tree rooting strategies should go in parallel with their potential physical barriers. Recent data products on global soil depth  
83 now enable to better constrain rooting depth in vegetation models across scales (Pelletier *et al.*, 2016).

84 Here we overcome the above mentioned limitations and present a new approach of diversifying tree rooting strategies of  
85 tropical plant functional types (PFTs) in the DGVM LPJmL4.0 (Lund-Potsdam-Jena managed Lands; Schaphoff *et al.*, 2018)  
86 which increases the ecological liability with the following aspects: 1) A global product of soil depth restricts the maximum  
87 tree rooting depth, 2) PFTs are sub-divided according to a broad spectrum of different possible tree rooting strategies with a  
88 range of maximum rooting depths between 0.5 and 18 m, 3) all sub-PFTs grow in competition and their individual  
89 performance determines dominance, 4) dominance is supported by best performing sub-PFTs increasing their establishment

90 rate, 5) sub-PFTs have to invest carbon into coarse roots, i.e. acknowledging the trade-off between growing deeper roots and  
91 allocating available carbon to other compartments (stem and leaf growth), and 6) sub-PFT roots are growing deeper over  
92 time depending on tree height. Given these new model developments we here re-evaluate the hypotheses that  
93 I) climate and soil depth determine dominant tree rooting strategies,  
94 II) tree rooting depth influences the distribution and dominance and  
95 III) diverse tree rooting strategies are key to explain rates of evapotranspiration and productivity  
96 of tropical evergreen forests in South America. Therefore, we compare several model versions of LPJmL4.0 differing in the  
97 above-mentioned model developments and evaluate simulated evapotranspiration, productivity, biomass and spatial  
98 distribution of evergreen and deciduous tree PFTs using different sources of validation data.

## 99 **2 Materials and Methods**

### 100 **2.1 The LPJmL4.0 model**

101 LPJmL4.0 is a process-based Dynamic Global Vegetation Model (DGVM) which simulates the surface energy balance,  
102 water fluxes, fire disturbance, carbon fluxes and stocks of the global land (Schaphoff et al., 2018a). Plant productivity is  
103 modelled on the basis of leaf-level photosynthesis responding to climatic and environmental conditions, atmospheric CO<sub>2</sub>  
104 concentration, canopy conductance, autotrophic respiration, phenology and management intensity. Fire disturbance is  
105 modelled using the simple fire module Glob-FIRM (Thonicke et al., 2001) which relates the length of the fire season to  
106 fractional annual area burnt. The model simulates 11 plant functional types (PFTs), 3 bioenergy functional types (BFTs) and  
107 12 crop functional types (CFTs), to represent average plants of natural vegetation, bioenergy plantations and agriculture,  
108 respectively. Three PFTs represent the natural vegetation of the tropics and sub-tropics namely the “tropical broadleaved  
109 evergreen tree” mainly representing tropical evergreen forest, the “tropical broadleaved deciduous tree” representing tropical  
110 dry forest and the woody component of savanna and “tropical herbs” representing the herbaceous layer in grasslands,  
111 savanna and forests. The standard spatial model resolution is a 0.5° x 0.5° longitude-latitude grid. For each grid cell the  
112 fractional coverage of bioenergy and agricultural BFTs and CFTs follows a prescribed land-use data set, whereas in the  
113 remaining grid-cell area natural PFTs grow in competition.

### 114 **2.2 A new tree rooting scheme for LPJmL4.0**

115 All changes made to LPJmL4.0 in order to simulate variable tree rooting strategies resulted in a new sub-version of  
116 LPJmL4.0 which we call LPJmL4.0-VR hereafter (where “VR” stands for “variable roots”). A detailed description of our  
117 modelling approach can be found in Appendix A.

118 For our purposes we extended the general maximum soil depth of 3 m in LPJmL4.0 to 20 m in LPJmL4.0-VR, but restrict it  
119 to local soil depth information at the spatial model resolution of 0.5° x 0.5°; Sect. 2.3.2. We applied the same basic scheme  
120 for vertical soil layer partitioning from LPJmL4.0 (Schaphoff et al., 2018a), in order to keep model differences small  
121 (Appendix A Sect. 1.1 & Table A1). We increased the amount of rooting strategies for each of the 2 tropical tree PFTs  
122 (broadleaved evergreen and broadleaved deciduous), by splitting each PFT into 10 sub-PFTs. Each of those 10 sub-PFTs  
123 was assigned a different maximum vertical distribution of fine roots throughout the soil column following classical  
124 allometric rules applied in LPJmL4.0 (Appendix A Sect. 1.3 & Figure A1). Those distributions were chosen in order to  
125 allow the sub-PFTs to reach different maximum rooting depths in discrete steps between 0.5 and 18 m (Table A2). We here  
126 refer to the depth at which the cumulated fine root biomass from the soil surface downwards amounts to 95% ( $D_{95\_max}$ ; Eq.  
127 A3). To account for additional carbon investments needed to grow deeper rooting systems we introduced two new carbon  
128 pools, namely root sapwood and root heartwood (Appendix A Sect. 1.4). Like stem sapwood in LPJmL4.0, also root  
129 sapwood in LPJmL4.0-VR needs to satisfy the assumptions of the pipe model (Shinozaki et al., 1964; Waring et al., 1982).

130 This implementation creates a trade-off between below-ground and above-ground carbon investment. To allow for dynamic  
131 root growth we implemented a logistic root growth function, which calculates a general maximum conceivable tree rooting  
132 depth depending on tree height (Appendix A Sect. 1.5), in approximation to the findings of Brum *et al.* (2019).  
133 Consequently, each sub-PFT shows a logistic growth of rooting depth which is dependent on the sub-PFT height and which  
134 saturates towards its specific  $D_{95\_max}$  (Fig. A2). Therefore, limitations of aboveground sub-PFT growth due to below-ground  
135 carbon investment of different tree rooting strategies (Sect. 2.2.4) are equal in the sapling phase of all sub-PFTs (starting  
136 from bare ground) but diverge with increasing sub-PFT height. In the case temporal root depths exceeds the grid-cell specific  
137 local soil depth (as prescribed by local soil depth information, see Sect. 2.3.2) all the respective fine root biomass exceeding  
138 this soil depth is transferred to the last soil layer matching this soil depth (see also Fig. 1 and Supplementary Video 1 for a  
139 visualization of new below-ground carbon pools and root growth in LPJmL4.0-VR under [http://www.pik-](http://www.pik-potsdam.de/~borissa/LPJmL4_VR/Supplementary_Video_1.pptx)  
140 [potsdam.de/~borissa/LPJmL4\\_VR/Supplementary\\_Video\\_1.pptx](http://www.pik-potsdam.de/~borissa/LPJmL4_VR/Supplementary_Video_1.pptx)).

141 To fully investigate the effects of 20 tropical sub-PFTs growing in competition we adjusted the original PFT establishment  
142 routine of LPJmL4.0 (Appendix A Sect. 1.6). The adjustments lead to a higher establishment rate for productive sub-PFTs  
143 relative to their spatial dominance and vice versa, without changing the overall establishment rate as originally set by  
144 Prentice *et al.* (1993). The adjusted establishment routine has the effect that non-viable sub-PFTs are outcompeted over time.  
145 Furthermore, we increased the universal and constant maximum background mortality rate of tree PFTs in LPJmL4.0-VR to  
146 7% in order to counter-balance increased survival rates and therefore biomass accumulation under enhanced water access  
147 (Appendix A Sect. 1.7).

## 148 **2.3 Model input data**

### 149 **2.3.1 Climate input data**

150 All versions of LPJmL used in this study (Sect. 2.4) were forced with 4 different climate inputs each delivering the climate  
151 variables air temperature, precipitation, long-wave and shortwave downward radiation at daily or monthly resolution:

152 1) WATCH Forcing Data (WFD) + WATCH Forcing Data methodology applied to ERAInterim data. A combination of the  
153 WATCH data set (Weedon *et al.*, 2011) and the WFDEI data set (Weedon *et al.*, 2014) as used in the ISIMIP project  
154 (<https://www.isimip.org/gettingstarted/input-data-bias-correction/details/5/>). This input data set is called WATCH+WFDEI  
155 hereafter.

156 2) Global Soil Wetness Project Phase 3 (GSWP3) (Kim *et al.*, no date; <http://hydro.iis.u-tokyo.ac.jp/GSWP3/index.html>).

157 3) NOAA Global Land Assimilation System version 2.0 (GLDAS, Rodell *et al.*, 2004).

158 4) Climate forcing as in Schaphoff *et al.* (2018) with monthly precipitation provided by the Global Precipitation Climatology  
159 Centre (GPCP Full Data Reanalysis version 7.0; (Becker *et al.*, 2013), daily mean temperature from the Climate Research  
160 Unit (CRU TS version 3.23, University of East Anglia Climatic Research Unit, 2015; Harris *et al.*, 2014), shortwave  
161 downward radiation and net downward radiation reanalysis data from ERA-Interim (Dee *et al.*, 2011), and number of wet  
162 days from (New *et al.*, 2000) used to allocate monthly precipitation to individual days.

163 This input data set is called CRU hereafter.

### 164 **2.3.2 Soil and sediment thickness**

165 For this study, we regridded a global 1 x 1 km soil and sediment thickness product (Pelletier *et al.*, 2016) to the 0.5° x 0.5°  
166 spatial resolution of LPJmL4.0-VR, set the global maximum value to 20 m according to the maximum soil depth chosen for  
167 LPJmL4.0-VR (Sect. 2.2 & Appendix A Sect. 1.1), and used the resulting map as grid cell specific model input (Fig. A3).  
168 Regridding was done using the software R (R Core Team, 2019) with the package “raster” (Hijmans and van Etten, 2016).  
169 We used the aggregate function to calculate the average value of all Pelletier *et al.* (2016) data entries falling into the coarser  
170 0.5° grid of LPJmL.

## 171 2.4 Model versions and simulation protocol

172 In order to investigate the impact of simulating variable rooting strategies and root growth, we employ 3 model versions of  
173 LPJmL in this study: 1) LPJmL4.0, 2) LPJmL4.0-VR, and 3) LPJmL4.0-VR-base. LPJmL4.0-VR-base has the same settings  
174 as LPJmL4.0-VR except variable rooting strategies, i.e. using the 2 rooting strategy parameterizations of LPJmL4.0  
175 (Appendix A Sect. 1.3) for the respective 10 sub-PFTs of the tropical broadleaved evergreen PFT and the tropical  
176 broadleaved deciduous PFT. We regard LPJmL4.0-VR-base as the baseline model of this study, because comparisons to  
177 LPJmL4.0-VR enable to investigate differences caused by the presence or absence of variable tree rooting strategies.

178 Each simulation was initialized with 5000 simulation years of spin up from bare ground without land-use by periodically  
179 cycling the first 30 years of the respective climate data set (1901-1930 for WATCH+WFDEI, GSWP3, CRU and 1948-1977  
180 for GLDAS) and using a pre-industrial atmospheric CO<sub>2</sub> level of 278 ppm. The first spin-up ensures that carbon pools and  
181 local distributions of PFTs and sub-PFTs are in equilibrium with climate (Schaphoff et al., 2018). In a second spin-up phase  
182 cycling the same 30 years of climate data, historical land-use and changing levels of atmospheric CO<sub>2</sub> concentration are  
183 introduced. The second spin-up starts in the year 1700 and ends with the first year available in each climate data set. Land-  
184 use is updated annually as described in Schaphoff et al. (2018). Before the year 1840 a constant pre-industrial atmospheric  
185 CO<sub>2</sub> concentration of 278 ppm is prescribed. After this year atmospheric CO<sub>2</sub> increases annually based on data of Tans and  
186 Keeling (2015) as described in Schaphoff et al. (2018). After the second spin up, transient simulations start with the first year  
187 available in each climate data set and end in 2100. Land-use and atmospheric CO<sub>2</sub> are consistently updated annually  
188 continuing to follow the same data sets as used in the second spin-up.

189 At the beginning of the first spin-up, all sub-PFTs in LPJmL4.0-VR and LPJmL4.0-VR-base have the same chance to  
190 establish, i.e. tree rooting strategies are uniformly distributed. During the spin-up simulations, local environmental filtering  
191 and competition in connection with PFT-dominance dependent establishment rates (Sect. 2.2 & Appendix A Sect. 1.6)  
192 determine which tree rooting strategies are best suited and which are outcompeted. Therefore, the transient simulations  
193 already start with distinct distributions of tree rooting strategies.

## 194 2.5 Model validation

### 195 2.5.1 Validation data

#### 196 *Regional biomass pattern*

197 For evaluation of simulated regional pattern of AGB we compare the results of the 3 LPJmL model versions used in this  
198 study to two remote sensing based biomass maps (Avitabile et al., 2016a; Saatchi et al., 2011) which were regridded to the  
199 spatial resolution of the LPJmL models. Data of Avitabile et al. (2016) was regridded using the software R (R Core Team,  
200 2019) with the package raster (Hijmans and van Etten, 2016). We used the aggregate function to calculate the average value  
201 of all Avitabile et al. (2016) data entries falling into the coarser 0.5° grid of LPJmL. RegridDED data of Saatchi et al. (2011)  
202 was taken from Carvalhais et al. (2014).

#### 203 *Local scale evapotranspiration and productivity*

204 To evaluate simulated local ET and net ecosystem exchange (NEE) of the 3 LPJmL versions used in this study, we compare  
205 Fluxnet eddy covariance measurements of ET at 7 sites and NEE at 3 sites across the study region (Bonal *et al.*, 2008;  
206 Saleska *et al.*, 2013, Table A3) to respective simulated rates of local ET and NEE. We used only 3 sites for NEE  
207 comparisons, because only those sites provided continuous data covering more than 2 years. Fluxnet data was downloaded  
208 from <https://fluxnet.fluxdata.org> (under DOI: [10.18140/FLX/1440032](https://doi.org/10.18140/FLX/1440032) and DOI: [10.18140/FLX/1440165](https://doi.org/10.18140/FLX/1440165)) in October 2017  
209 and from [https://daac.ornl.gov/LBA/guides/CD32\\_Brazil\\_Flux\\_Network.html](https://daac.ornl.gov/LBA/guides/CD32_Brazil_Flux_Network.html) in November 2019.

#### 210 *Continental scale gridded evapotranspiration products and selection of regions*

211 To evaluate the simulated ET over large regions and during a long period (1981-2010), we use three global gridded datasets:  
212 Global Land Data Assimilation System Version 2 (Rodell et al., 2004), ERA-Interim/Land (ERA-L, Balsamo *et al.*, 2015)  
213 and Global Land Evaporation Amsterdam Model v3.2 (GLEAM, Miralles *et al.*, 2011; Martens *et al.*, 2017).  
214 GLDAS and ERA-L are reanalysis products, meaning that they are land surface models forced with meteorological data that  
215 has been corrected with observations to give better estimates of land surface variables. The selection of these two products is  
216 based on the study of Sörensson and Ruscica (2018), who found that they have a better performance over South America  
217 than other reanalysis and satellite-based ET products. GLDAS uses the land surface model Noah (Ek et al., 2003) forced by  
218 Princeton meteorological dataset version 2.2 (Sheffield et al., 2006). The soil depth of Noah is 2 m and the model uses four  
219 soil layers and vegetation data from University of Maryland (<http://glcf.umd.edu/data/landcover/>). ERA-L uses the land  
220 surface model HTESSEL (Hydrology-Tiled ECMWF Scheme for Surface Exchanges over Land, Balsamo *et al.*, 2009)  
221 forced by ERA-Interim atmospheric data with a GPCP based correction of monthly precipitation. The soil depth of ERA-L  
222 is 2.89 m, the model uses four soil layers and vegetation data from ECOCLIMAP (Masson et al., 2003).  
223 GLEAM uses the Priestley-Taylor equation to estimate the potential ET and a set of algorithms with meteorological and  
224 vegetation satellite data as input to calculate the actual ET. The version used here, GLEAMv3.2a (Martens *et al.*, 2017,  
225 downloaded from <https://www.gleam.eu/#downloads>) uses precipitation input from MSWEP v1.0 (Beck et al., 2017),  
226 vegetation cover from the MODIS product MOD44B, remotely sensed Vegetation Optical Index from CCI-LPRM (Liu et  
227 al., 2013) and assimilates soil moisture from both remote sensing (ESA CCI SM v2.3, Liu *et al.*, 2012) and land-reanalysis  
228 (GLDAS Noah, Rodell *et al.*, 2004). The original spatio-temporal resolution of GLDAS and GLEAM is 0.25° x 0.25° while  
229 for ERA-L it is 0.75° x 0.75°. Monthly time series were calculated from daily values for the three datasets. Hereafter, we use  
230 the short names GLDAS, ERA-L and GLEAM for the described reference datasets.

231 For the temporal analysis of ET we used five climatological regions across the study area: Northern South America (NSA),  
232 Equatorial Amazon West (EQ W), Equatorial Amazon East (EQ E), Southern Amazon (SAMz), and South American  
233 Monsoon System region (SAMS) (see Fig. 3f). These regions result from a K-means clustering analysis of the annual cycles  
234 of the main drivers of ET: precipitation and surface net radiation (for details see Sörensson and Ruscica, 2018). Additionally  
235 we divided the large EQ region used by Sörensson and Ruscica (2018) in two smaller (EQ W and EQ E) at 60°W, since this  
236 is the approximate division between regimes that have a maximum climatological water deficit (MCWD; Sect. 2.5.3) of  
237 around -200 mm per year (EQ W), and of around -500 mm per year (EQ E).

### 238 *Spatial distribution of vegetation types*

239 To evaluate the simulated regional distribution of simulated biome types of the 3 LPJmL versions we compare our results to  
240 satellite-derived vegetation composition maps from ESA Land cover CCI V2.0.7 (Li et al., 2018) which were reclassified to  
241 the PFTs of LPJmL from Forkel *et al.* (2014). In this dataset PFT dominance is indicated by foliage projected cover (FPC)  
242 which is also a standard output variable of the 3 LPJmL model versions allowing a direct comparison to model results.

### 243 *Spatial pattern of rooting depth*

244 We compare regional patterns of mean rooting depth simulated with LPJmL4.0-VR to a maximum depth of root water  
245 uptake map (Fan et al., 2017) which was regridded to the 0.5° x 0.5° spatial resolution of LPJmL4.0-VR. This product was  
246 inversely modelled by taking the dynamically interacting variables soil water supply and plant water demand into account. In  
247 Fan et al. (2017) supply was based on climate, soil properties and topography and demand of plant transpiration deduced  
248 from remotely sensed reanalysis of atmospheric water fluxes and leaf area index (LAI) data.

## 249 **2.5.2 Validation metrics**

250 All statistical evaluations of model results were based on 1) Pearson Correlation and 2) normalized mean squared error  
251 (NME; Kelley *et al.*, 2013). NME is calculated as:

252 
$$NME = \frac{\sum_{i=1}^N |y_i - x_i|}{\sum_{i=1}^N |x_i - \bar{x}|}$$
 Eq. (1)

253 where  $y_i$  is the simulated and  $x_i$  the reference value in the grid cell or time step  $i$ .  $\bar{x}$  is the mean reference value. NME takes  
 254 the value 0 at perfect agreement, 1 when the model performs as well as the reference mean and values  $> 2$  indicate complete  
 255 disagreement.

### 256 2.5.3 Maximum cumulative water deficit as indicator of seasonal water stress

257 To analyse and explain the geographical pattern of rooting depth, ET and productivity we use the maximum cumulative  
 258 water deficit (MCWD) as an independent indicator of potential seasonal water demand of vegetation. MCWD is a widely  
 259 used indicator for seasonal water stress of tropical and sub-tropical forests in South America (Aragão et al., 2007; Lewis et  
 260 al., 2011; Malhi et al., 2009). MCWD captures the seasonal difference of ET and precipitation in a cumulative way and  
 261 therefore comprises dry season strength and duration. Here we calculate MCWD on a monthly basis. Therefore, we first  
 262 calculate the cumulative water deficit  $CWD_n$  of each month  $n$  as:

263 
$$CWD_n = CWD_{n-1} - PET_n + P_n$$
 Eq. (2)

264 where PET is the potential monthly ET and P the monthly sum of precipitation. CWD is constrained to values  $\leq 0$  and is set  
 265 to 0 at the end of each hydrological year, here the last day of September, as in Lewis *et al.* (2011). We use  $P$  from climate  
 266 input used for model forcing (Sect. 2.3.1) and PET as it is simulated by LPJmL4.0 (Schaphoff et al., 2018a) which is only  
 267 dependent on net surface radiation and air temperature, therefore remaining an explanatory variable independent of  
 268 vegetation dynamics. We chose this PET instead of using the commonly used constant ET of 100 mm/month to calculate  
 269 CWD (Aragão et al., 2007; Lewis et al., 2011; Malhi et al., 2009), because in this way, the CWD better corresponds to the  
 270 actual climatological conditions in the different LPJmL model versions used in this study (Sect. 2.4). MCWD is then  
 271 calculated as:

272 
$$MCWD_y = \min(CWD_{October,y-1}, \dots, CWD_{September,y})$$
 Eq. (3)

273 where  $y$  indicates the calendrical year.

## 274 3 Results

### 275 3.1 Regional pattern of tree rooting strategies

276 In LPJmL4.0-VR the contribution of each tree rooting strategy to the overall net primary productivity (NPP) appears highly  
 277 dependent on local environmental conditions.

278 Based on the information of how much NPP each sub-PFT contributes in each grid cell, we derived maps of mean rooting  
 279 depth over the whole study region for the time span 2001-2010 for each climate input used in this study (Fig. 2). Fig. 2  
 280 shows the mean of the actually achieved  $D_{95}$  of each sub-PFT (evergreen and deciduous combined) weighted by the  
 281 respective relative NPP contribution of each sub-PFT to total forest NPP (we call  $\overline{D_{95}}$ , hereafter). Therefore, the regional  
 282 pattern of  $\overline{D_{95}}$  reflects the effects of climate and soil depth. A general East to West gradient of  $\overline{D_{95}}$  over the Amazon region  
 283 follows climatic gradients of precipitation and MCWD (Fig. B1-B2), while soil depth (Fig. A3) constrains  $\overline{D_{95}}$  especially in  
 284 the South-Eastern Amazon. In general, areas with higher mean annual rainfall and weaker dry season show lower  $\overline{D_{95}}$  and  
 285 vice versa (please also see Fig. B3 for a detailed exemplary comparison of sub-PFT NPP for 2 grid cells with contrasting  
 286 climate conditions). This pattern holds true under all climate inputs, with some minor local differences and is in line with an  
 287 inversely modelled global gridded product of maximum depth of root water uptake (MDRU in Fan et al. 2017).  
 288 Nevertheless, we find considerable absolute differences between MDRU and  $\overline{D_{95}}$  (Fig. B4), which can easily emerge from  
 289 different model settings and assumptions, e.g. related to differences in spatial model resolution, simulated water percolation  
 290 and underlying vegetation features.

291 Focussing on the climatological clusters (Sect. 2.5.1 and Fig. 3f) under CRU climate input, the western Amazon (EQ W),  
292 with a MAP of 2708 mm and mean MCWD of -163 mm, displays an overall mean  $\overline{D_{95}}$  of 1.14 m and a maximum of 5.47 m,  
293 despite considerably deeper soils present. In this cluster Fan et al. (2017) find a respective mean and maximum MDRU of  
294 1.26 and 17.95 m. In the Northern, Western and Southern Amazon clusters (NSA, EQ E, SAMz) with lower MAP of 2299,  
295 2190 and 2035 mm and considerably lower MCWD of -488, -438 and -497 mm, respectively, mean  $\overline{D_{95}}$  increases to 2.32,  
296 3.20 and 2.68 m, respectively (mean MDRU of 1.85, 2.84 and 3.28 m). Here, maximum  $\overline{D_{95}}$  values respectively reach 11.97,  
297 11.27 and 9.04 m (maximum MDRU of 14.28, 13.47 m and 16.57 m). In the monsoon dominated region (SAMS) displaying  
298 the lowest MAP of 1449 mm and MCWD of -649 mm, mean  $\overline{D_{95}}$  decreases to 1.37 m (mean MDRU 2.61 m). The maximum  
299  $\overline{D_{95}}$  of this region reaches 11.17 m located at the border to SAMz (maximum MDRU 49.37 m).

300 The regional simulation of  $\overline{D_{95}}$  also allows us to generalize which tree rooting strategies occupy which climate space. Using  
301 MCWD and MAP to define a climate space we find a clear adjustment of  $\overline{D_{95}}$  (Fig. B5). A core region with deep-rooted  
302 forests (mean  $\overline{D_{95}} > 4$  m) is found where MCWD ranges between -1300 and -400 and where MAP is at least 1500 mm (see  
303 also maps of MCWD and MAP in Fig. B1-B2). This core region is surrounded by a small band of medium rooting depth  
304 forests (mean  $\overline{D_{95}} \sim 2-4$  m). Rather shallow-rooted forests (mean  $\overline{D_{95}} < 2$  m) are found in increasingly drier climates where  
305 MAP is less than 1000 mm and in more seasonal climates where MCWD is below -500 mm. Shallow-rooted forests are also  
306 simulated in very wet conditions where MCWD is greater than -300 mm and MAP is 1200 mm or higher.

### 307 **3.2 Evapotranspiration and productivity**

308 The climatological clusters within the Amazon region which undergo the strongest dry season (EQ E and SAMz) show the  
309 largest differences between simulations with variable (LPJmL4.0-VR) and constant tree rooting strategies (LPJmL4.0-VR-  
310 base and LPJmL4.0). In those clusters LPJmL4.0-VR shows a significant higher agreement with validation data (Fig. 3c, d  
311 and Table B3). Agreement is largest for EQ E where NME and  $r^2$  show values of 0.62 and 0.91, respectively, whereas  
312 constant rooting systems in the other two models lead to values of NME  $\geq 1.92$  and  $r^2 \leq 0.21$  (Table B3). In NSA and EQ  
313 W model differences are less pronounced as annual precipitation deficits are lower and deep rooting systems play a lesser  
314 role. Still, variable rooting systems lead to noticeably higher agreement in NSA between January and April (Fig. 3a), where  
315 monthly precipitation is lower compared to the rest of the year. In the monsoon dominated cluster SAMS outside the  
316 Amazon region (Fig. 3e), model differences are least pronounced, since shallow rooting forests dominate this area in  
317 LPJmL4.0-VR (Fig. 2) which are very similar to the forests with constant tree rooting strategies in the other 2 model  
318 versions.

319 Results of regional ET are in line with results of site-specific ET. On the local level, variable tree rooting strategies of  
320 LPJmL4.0-VR lead to a major improvement in reproducing measured Fluxnet NEE and ET (Appendix B Sect. 1.1 & Fig B6-  
321 B7), increasing the confidence of regional modelling results.

### 322 **3.3 Distribution of plant functional types**

323 The simulated relative dominance of tropical tree PFTs across the study area differs substantially between model versions  
324 (Fig. 4). In simulations with LPJmL4.0, more than half of the grid cells show the evergreen and deciduous PFTs equally  
325 dominant (Fig. 4g-h). Only in areas outside tropical moist climate regions the model tends towards a dominance of the  
326 deciduous PFT, whereas e.g. in the Amazon region, the evergreen and deciduous PFTs co-exist in almost equal abundance.  
327 These patterns strongly differ from satellite-derived geographical PFT distributions (Fig. 4a-b) and therefore yield in  
328 respective comparisons the highest NME values among all models (Table B4). In contrast LPJmL4.0-VR and LPJmL4.0-  
329 VR-base show clear dominance patterns of both tropical tree PFTs across the study area (Fig. 4c-f). Nevertheless, differences  
330 between LPJmL4.0-VR and LPJmL4.0-VR-base are quite substantial. In LPJmL4.0-VR-base the tropical evergreen PFT  
331 dominates the North-Western Amazon region only, negligibly extending further than the borders of climatological clusters



332 NSA and EQ W combined. Beyond these borders the tropical deciduous PFT dominates (Fig. 4e-f). In contrast, in  
333 LPJmL4.0-VR (Fig. 4e-f) the evergreen tree PFT dominates the entire Amazon region including EQ E and SAMz, and the  
334 deciduous PFT is pushed towards drier and more seasonal climate (including parts of SAMS). Therefore, LPJmL4.0-VR  
335 yields the lowest NME values in comparison to satellite-derived PFT distributions (Table B4).

## 336 4 Discussion

### 337 4.1 Climate and soil depth determine dominant tree rooting strategies

338 The geographical patterns of simulated  $\overline{D_{95}}$  are very similar under 4 different climate input data sets (Fig. 2). This gives  
339 confidence to the general robustness of our results and modelling approach as differences in climate data do not lead to  
340 substantially different model behaviour. This is further supported by similar regional rates of ET simulated under the  
341 different climate data inputs (Fig. 3).

342 Simulated  $\overline{D_{95}}$  (Fig. 2) clearly follows climate gradients and soil depth found in the study region (Fig. A3, B2-B3). Here,  
343 MAP and MCWD can serve as explanatory variables of simulated  $\overline{D_{95}}$  (Fig. B5). These findings are in line with the general  
344 ecological expectation and former studies that seasonal water depletion of upper soil layers, as a combination of annual  
345 precipitation and dry season length and strength, is positively correlated with the rooting depth of tropical evergreen trees  
346 (Baker et al., 2009; Ichii et al., 2007; Kleidon and Heimann, 1998, 1999). We also find lower thresholds for MAP and  
347 MCWD where  $\overline{D_{95}}$  strongly decreases again (Fig. B5) which can be explained by different mechanisms leading to a regime  
348 shift from the evergreen to the deciduous tree PFT as discussed below (see Sect. 4.2).

349 To evaluate our model results against empirical data, we checked the data availability on maximum rooting depth across  
350 South America in the TRY database (Kattge *et al.*, 2020; data downloaded September 2019). As it is also shown in Fan *et al.*  
351 (2017) we found the number of sites within the TRY data base where maximum rooting depth has been measured in South  
352 America to be very low. Moreover, the number of data entries per site appeared very small, where 33 TRY sites falling  
353 within our study area showed a mean of 9 and a median of 6 data entries, while 15 sites showed  $\leq 5$  data entries. Therefore,  
354 we decided to not include site specific comparisons of rooting depth as it is not clear how representative these measurements  
355 are for the local forest communities. More research is necessary to increase the number of observation sites and improve the  
356 empirical basis of field-based rooting depth to allow for site-specific model evaluation. Nevertheless, as shown in Fan *et al.*  
357 (2017) measured site-specific maximum rooting depth across the Amazon region expectedly follows the known climatic  
358 gradient (Fig. B1-B2). The same holds true for the inversely modelled MDRU of Fan *et al.* (2017; we show in Fig. B4),  
359 which gives confidence to our results.

### 360 4.2 Rooting depth influences the distribution, dominance and biomass of tropical plant functional types

361 In all 3 model versions used in this study the same land-use is applied (Sect. 2.4), which shapes the geographical extent and  
362 maximum dominance of natural vegetation in our results. This is why FPC maps of all model versions show the shape of the  
363 Amazon region as a distinct pattern (Fig 4), even though it is less visible for LPJmL4.0-VR-base and one has to consider  
364 both tropical tree PFTs at the same time (Fig. 4e-f). Within the Amazon region, LPJmL4.0 simulates a similar dominance of  
365 the evergreen and deciduous PFT (Fig. 4g-h) which contradicts evaluation data (Fig. 4a-b) and indicates a similar  
366 performance of the 2 PFTs or missing mechanisms rewarding a better performance over time. We here find that introducing  
367 a performance dependent tree establishment rate (Sect. 2.2 and Appendix A Sect. 1.6) clearly resolves this issue. This feature  
368 produces clear dominance pattern of either PFT in LPJmL4.0-VR and LPJmL4.0-VR-base. Apparently, by rewarding better  
369 performance, variable tree rooting strategies (LPJmL4.0-VR) become necessary to reproduce the dominance of the evergreen  
370 PFT throughout the Amazon region (Fig. 4e-f). To remain superior in drier and more seasonal environments in the South to  
371 South-Eastern Amazon region the evergreen PFT needs to access deep water by adjusting its rooting depth (Fig. 2). Clearly,

372 this adjustment of rooting depth is only possible within a certain climatic envelope. Below certain thresholds of MAP  
373 (around 1000 mm) and MCWD (around -500 mm) mean  $\overline{D_{95}}$  decreases again (Fig. B5), which coincides with a transition  
374 from the evergreen to the deciduous PFT. Those thresholds are similar to thresholds between evergreen forests and savanna  
375 found by e.g. Malhi *et al.* (2009) at an annual precipitation of 1500 mm and at an MCWD of -300 mm. The substantially  
376 lower MCWD value found in our study can be explained by the differences in calculating CWD. While Malhi *et al.* (2009)  
377 assume a constant rate of ET per month of 100 mm, we use the monthly variable PET (Sect. 2.5.3). Since PET often is  
378 significantly higher than 100 mm our monthly CWD and therefore MCWD values are respectively lower.

379 Similarly to Malhi *et al.* (2009), Staver, Archibald and Levin (2011) find that the climatic thresholds for evergreen forest are  
380 not very distinct and savanna can simultaneously be found in a climatic range around the mean threshold. The authors  
381 ascribe this forest-savanna bi-stability to climate-fire-vegetation feedbacks. Many recent studies investigating potential  
382 forest-savanna bi-stability and tipping points of forests in and around the Amazon region rely solely on such climatic ranges  
383 of tropical biomes (Hirota *et al.*, 2011; Wuyts, Champneys and House, 2017; Zemp *et al.*, 2017; Staal *et al.*, 2018; Ciemer *et al.*,  
384 2019). The results of LPJmL4.0-VR show that knowledge on local tree root adaptations is another important explanatory  
385 variable of vegetation cover reducing the uncertainty and width of anticipated climatic ranges where vegetation cover could  
386 be bi-stable. These findings are supported by a recent study that finds rooting depth more crucial than fire dynamics for  
387 explaining PFT dominance in South America (Langan *et al.*, 2017).

388 Whether the transition between the evergreen and deciduous tree PFT for the thresholds of MAP and MCWD we find with  
389 LPJmL4.0-VR is mainly caused by (a) environmental filtering (including vegetation-fire feedbacks) of deep tree rooting  
390 strategies, (b) their competitive exclusion by shallow rooted deciduous sub-PFTs together with the tropical herbaceous PFT  
391 (Fig. B8), or most probably a combination of both is yet to be determined. Given that we used the most simplistic fire  
392 module of LPJmL (GlobFirm; Thonicke *et al.*, 2001) and current land-use input to allow model evaluation against remotely  
393 sensed data in this study, investigating the natural mechanisms of tropical PFT shifts should be in the focus of further  
394 studies.

395 Regardless of the mechanisms that eventually lead to a PFT shift, we can state that neither costs for deep root investment nor  
396 a heterogeneous pattern of soil depth across the study region disproves that locally adapted tree rooting depth is key to  
397 explain the current geographical distribution of tropical evergreen forests in South-America. Given the large differences  
398 between LPJmL4.0-VR and LPJmL4.0-VR-base (Fig. 4) it is clear that in roughly half of the Amazon region the carbon  
399 balance of the evergreen PFT is superior to the deciduous PFT only when investing substantial amounts of carbon into  
400 deeper roots, i.e. belowground biomass (; Fig. B9). On the one hand this investment has a direct negative effect on  
401 productivity, because during growth the allocation of assimilated carbon shifts towards respiring belowground biomass ,  
402 while investments into productive AGB (Fig. B10) need to be reduced. On the other hand, drier and more seasonal  
403 environments show less cloud cover during the dry season (Nemani *et al.*, 2003), enhancing photosynthesis in this time of  
404 the year which increases productivity as long as water access is assured (Costa *et al.*, 2010; Wu *et al.*, 2016). The trade-off  
405 between AGB and BGB investment most probably leads to a more homogenous AGB pattern across the Amazon region with  
406 similar values over a wide climatic range (compare EQ E and SAMz in Fig. B10c-e).

#### 407 **4.3 Diverse tree rooting strategies improve simulated evapotranspiration and productivity**

408 LPJmL4.0-VR simulates rates of local ET and NEE which reasonably match respective measurements at different Fluxnet  
409 sites throughout the Amazon region (Fig. B6-B7), even though we run the model with regionally gridded instead of locally  
410 measured climate data. While potentially lacking information on local short-term weather events, gridded climate input still  
411 seems to be sufficient to capture broad seasonal signals for our comparisons on a monthly basis. This increases the  
412 confidence in our results also on a regional scale.

413 Across large parts of the Amazon region variable tree rooting strategies decrease the intra-annual variability of ET and  
414 maintain high rates of NEE and ET during the dry season in accordance with the intra-annual trends suggested by evaluation  
415 data (Fig. 3, B6-B7). More than that simulated rates of ET and productivity can peak during the dry season, e.g., in EQ E  
416 which has been explained by increased solar radiation during this time of the year (Nemani et al., 2003; da Rocha et al.,  
417 2004). Especially, in EQ E and SAMz at least parts of the forest area must have access to sufficient water in the model and in  
418 reality (Costa et al., 2010; Wu et al., 2016). Given that LPJmL4.0-VR and LPJmL4.0-VR-base are essentially identical  
419 models with the same soil depth input and subsequent hydrology over the whole soil column, their differences in simulated  
420 ET and NEE must emerge from their only difference which is the amount of simulated tree rooting strategies. Therefore,  
421 local root adaptations in LPJm4.0-VR can be regarded as a buffer against seasonal precipitation deficits by usage of deep  
422 water (exemplary shown in large detail for the Fluxnet Site STM K67 in Fig. B11).

423 We can here quantify this water access for the first time on the basis of carbon investment and return, and limited by spatial  
424 heterogeneous soil depth. Without limits to rooting depth in the form of local soil depth (e.g. by applying a universal soil  
425 depth of 20 m) and below-ground carbon investment, seasonally dry climatological clusters would potentially shift towards  
426 deeper rooted sub-PFT dominance, consequently leading to an overestimation of ET rates. Therefore, we argue that both  
427 factors are of great importance to explain regional rates of ET. This also means that forests in the same climatological cluster  
428 contribute very differently to the overall ET and therefore to moisture recycling across South America. We can here  
429 mechanistically explain this coherence as we show for the first time on the regional scale how PFTs with variable tree  
430 rooting strategies adjust to local environmental conditions and in return lead to simulated rates of ET very close to validation  
431 data (Fig. 3, B6). The heterogeneous picture of  $\overline{D_{95}}$  we find (Fig. 2) might provide a direct guideline where to put emphasis  
432 on forest conservation to maintain continental scale moisture recycling, as  $\overline{D_{95}}$  directly scales with rates of ET.

433 Being able to mechanistically reproduce and explain the broad-scale stabilization of water fluxes into the atmosphere has  
434 wide implications for DGVM modelling frameworks and simulation of ET as moisture input to the atmosphere in Earth  
435 System Models (ESMs). Our approach can help to better quantify the role of forests for local-to-continental scale moisture  
436 recycling and to project the fate of forests under future climate and land-use change. The approach presented here is easily  
437 applicable for a wide range of DGVMs and ESMs which simulate fine root distribution in a similar way as the LPJmL model  
438 family (based on Jackson *et al.*, 1996). A first and easy to implement step for other models could be to prescribe the relative  
439 fine root distribution in a spatial explicit way in accordance to  $\overline{D_{95}}$  presented in this study.

## 440 5 Conclusions

441 In this paper we reconfirm the hypotheses that climate and soil depth determine dominant tree rooting strategies (hypothesis  
442 I), tree rooting depth is key to explain the distribution and dominance (hypothesis II) as well as, evapotranspiration and  
443 productivity rates of tropical evergreen forests in South America (hypothesis III), even when the competition of tree rooting  
444 strategies and carbon investment into gradually growing roots are considered. In fact our findings suggest that roughly half  
445 of the evergreen forests in the Amazon region depend on investments into rooting systems which go deeper than the standard  
446 average PFT parameterization based on literature allows for. Those deep root systems can be regarded as a buffer against  
447 seasonal precipitation deficits by usage of deep water and keep rates of ET and productivity at high levels throughout the  
448 year.

449 A major advance of the new sub-model version LPJmL4.0-VR is that simulations start with uniform input distributions of  
450 tree rooting strategies in each location which shape into a distribution of abundance driven by local environmental filtering  
451 and competition. Therefore, these distributions are not a pre-selected input, but an emergent simulation output.

452 The new model features enable to introduce local tree rooting depth as a key explanatory variable in future studies dealing  
453 with bi-stability of potential forest cover in tropical regions. Generally, we are convinced that our approach is of high

454 importance to all modelling frameworks of DGVMs and Earth System Models (ESMs) aiming at quantifying continental  
455 scale moisture recycling, forest tipping points and resilience. So far, the importance of local-scale tree root adaptations for  
456 regional-scale ecosystem functions underlines the need to protect this below-ground functional diversity not only in the  
457 scope of future global change.

## 458 **6 Code availability**

459 The model code of LPJmL4.0-VR can be found under <https://doi.org/10.5281/zenodo.4709250> and should be cited as  
460 Sakschewski et al. (2021a). The model code of standard LPJmL4.0 can be found under Schaphoff et al. (2018b).

## 461 **7 Data availability**

462 All output data of LPJmL4.0-VR, LPJmL4.0-VR-base and LPJmL4.0 analysed in this study can be found under  
463 <https://doi.org/10.5281/zenodo.4709166> and should be cited as Sakschewski et al. (2021b).

## 464 **8 Author contribution**

465 All authors helped in conceptualizing the model. BS and WvB developed the model code. BS, WvB, MD, AS, RR, FL, MB,  
466 SB, MH, RO, KT conceived the simulation experiments and BS carried them out. BS, MD, AS, RR and JH analysed model  
467 output data. BS prepared the manuscript with contributions from all co-authors.

## 468 **9 Competing interests**

469 The authors declare that they have no conflict of interest.

## 470 **10 Acknowledgements**

471 BS and KT acknowledge funding from the BMBF- and Belmont Forum-funded project “CLIMAX: Climate services through  
472 knowledge co-production: A Euro-South American initiative for strengthening societal adaptation response to extreme  
473 events”, FKZ 01LP1610A. MD is funded by the DFG/FAPESP within the IRTG 1740/TRP 2015/50122-0. MH is supported  
474 by a grant from Instituto Serrapilheira/Serra 1709-18983. A. Sörensson and R. Ruscica acknowledge support from PICT-  
475 2018-02511 (ANPCyT, Argentina). This work used eddy covariance data acquired and shared by the FLUXNET  
476 community, including these networks: AmeriFlux, AfriFlux, AsiaFlux, CarboAfrica, CarboEuropeIP, CarboItaly,  
477 CarboMont, ChinaFlux, Fluxnet-Canada, GreenGrass, ICOS, KoFlux, LBA, NECC, OzFlux-TERN, TCOS-Siberia, and  
478 USCCC. The ERA-Interim reanalysis data are provided by ECMWF and processed by LSCE. The FLUXNET eddy  
479 covariance data processing and harmonization was carried out by the European Fluxes Database Cluster, AmeriFlux  
480 Management Project, and Fluxdata project of FLUXNET, with the support of CDIAC and ICOS Ecosystem Thematic  
481 Center, and the OzFlux, ChinaFlux and AsiaFlux offices.

## 482 **11 References**

483 Allen, C. D., Breshears, D. D. and McDowell, N. G.: On underestimation of global vulnerability to tree mortality and forest  
484 die-off from hotter drought in the Anthropocene, *Ecosphere*, 6(8), 1–55, doi:10.1890/ES15-00203.1, 2015.  
485 Aragão, L. E. O. C., Malhi, Y., Roman-Cuesta, R. M., Saatchi, S., Anderson, L. O. and Shimabukuro, Y. E.: Spatial patterns  
486 and fire response of recent Amazonian droughts, *Geophys. Res. Lett.*, 34(7), 1–5, doi:10.1029/2006GL028946, 2007.

487 Arnold, J. G., Williams, J. R., Nicks, A. D. and Sammons, N. B.: SWRRB; a basin scale simulation model for soil and water  
488 resources management., SWRRB; a basin scale Simul. Model soil water Resour. Manag., 1990.

489 Avitabile, V., Herold, M., Heuvelink, G. B. M., Lewis, S. L., Phillips, O. L., Asner, G. P., Armston, J., Ashton, P. S., Banin,  
490 L., Bayol, N., Berry, N. J., Boeckx, P., de Jong, B. H. J., Devries, B., Girardin, C. A. J., Kearsley, E., Lindsell, J. A., Lopez-  
491 Gonzalez, G., Lucas, R., Malhi, Y., Morel, A., Mitchard, E. T. A., Nagy, L., Qie, L., Quinones, M. J., Ryan, C. M., Ferry, S.  
492 J. W., Sunderland, T., Laurin, G. V., Gatti, R. C., Valentini, R., Verbeeck, H., Wijaya, A. and Willcock, S.: An integrated  
493 pan-tropical biomass map using multiple reference datasets, *Glob. Chang. Biol.*, 22(4), 1406–1420, doi:10.1111/gcb.13139,  
494 2016a.

495 Avitabile, V., Herold, M., Heuvelink, G. B. M., Lewis, S. L., Phillips, O. L., Asner, G. P., Armston, J., Ashton, P. S., Banin,  
496 L., Bayol, N., Berry, N. J., Boeckx, P., de Jong, B. H. J., Devries, B., Girardin, C. A. J., Kearsley, E., Lindsell, J. A., Lopez-  
497 Gonzalez, G., Lucas, R., Malhi, Y., Morel, A., Mitchard, E. T. A., Nagy, L., Qie, L., Quinones, M. J., Ryan, C. M., Ferry, S.  
498 J. W., Sunderland, T., Laurin, G. V., Gatti, R. C., Valentini, R., Verbeeck, H., Wijaya, A. and Willcock, S.: An integrated  
499 pan-tropical biomass map using multiple reference datasets, *Glob. Chang. Biol.*, 22(4), 1406–1420, doi:10.1111/gcb.13139,  
500 2016b.

501 Baker, I. T., Prihodko, L., Denning, A. S., Goulden, M., Miller, S. and Da Rocha, H. R.: Seasonal drought stress in the  
502 amazon: Reconciling models and observations, *J. Geophys. Res. Biogeosciences*, 114(1), 1–10, doi:10.1029/2007JG000644,  
503 2008.

504 Baker, I. T., Prihodko, L., Denning, A. S., Goulden, M., Miller, S. and Da Rocha, H. R.: Seasonal drought stress in the  
505 amazon: Reconciling models and observations, *J. Geophys. Res. Biogeosciences*, 114(1), 1–10, doi:10.1029/2007JG000644,  
506 2009.

507 Balsamo, G., Viterbo, P., Beijaars, A., van den Hurk, B., Hirschi, M., Betts, A. K. and Scipal, K.: A revised hydrology for  
508 the ECMWF model: Verification from field site to terrestrial water storage and impact in the integrated forecast system, *J.*  
509 *Hydrometeorol.*, 10(3), 623–643, doi:10.1175/2008JHM1068.1, 2009.

510 Balsamo, G., Albergel, C., Beljaars, A., Boussetta, S., Brun, E., Cloke, H., Dee, D., Dutra, E., Munõz-Sabater, J.,  
511 Pappenberger, F., De Rosnay, P., Stockdale, T. and Vitart, F.: ERA-Interim/Land: A global land surface reanalysis data set,  
512 *Hydrol. Earth Syst. Sci.*, 19(1), 389–407, doi:10.5194/hess-19-389-2015, 2015.

513 Beck, H. E., Van Dijk, A. I. J. M., Levizzani, V., Schellekens, J., Miralles, D. G., Martens, B. and De Roo, A.: MSWEP: 3-  
514 hourly 0.25° global gridded precipitation (1979-2015) by merging gauge, satellite, and reanalysis data, *Hydrol. Earth Syst.*  
515 *Sci.*, 21(1), 589–615, doi:10.5194/hess-21-589-2017, 2017.

516 Becker, A., Finger, P., Meyer-Christoffer, A., Rudolf, B., Schamm, K., Schneider, U. and Ziese, M.: A description of the  
517 global land-surface precipitation data products of the Global Precipitation Climatology Centre with sample applications  
518 including centennial (trend) analysis from 1901-present, *Earth Syst. Sci. Data*, 5(1), 71–99, doi:10.5194/essd-5-71-2013,  
519 2013.

520 Best, M. J., Pryor, M., Clark, D. B., Rooney, G. G., Essery, R. . L. H., Ménard, C. B., Edwards, J. M., Hendry, M. A.,  
521 Porson, A., Gedney, N., Mercado, L. M., Sitch, S., Blyth, E., Boucher, O., Cox, P. M., Grimmond, C. S. B. and Harding, R.  
522 J.: The Joint UK Land Environment Simulator (JULES), model description – Part 1: Energy and water fluxes, *Geosci. Model*  
523 *Dev.*, 4(3), 677–699, doi:10.5194/gmd-4-677-2011, 2011.

524 Bonal, D., Bosc, A., Ponton, S., Goret, J., Burban, B., Gross, P., Bonnefonds, J. M., Elbers, J. A., Longdoz, B., Epron, D.,  
525 Guehl, J. and Granier, A.: Impact of severe dry season on net ecosystem exchange in the Neotropical rainforest of French  
526 Guiana, , 14(8), 1917–1933 [online] Available from: <https://edepot.wur.nl/1900>, 2008.

527 Brum, M., Vadeboncoeur, M. A., Ivanov, V., Asbjornsen, H., Saleska, S., Alves, L. F., Penha, D., Dias, J. D., Aragão, L. E.  
528 O. C., Barros, F., Bittencourt, P., Pereira, L. and Oliveira, R. S.: Hydrological niche segregation defines forest structure and  
529 drought tolerance strategies in a seasonal Amazon forest, *J. Ecol.*, 107(1), 318–333, doi:10.1111/1365-2745.13022, 2019.

530 Brunner, I., Herzog, C., Dawes, M. A., Arend, M. and Sperisen, C.: How tree roots respond to drought, *Front. Plant Sci.*,  
531 6(JULY), 1–16, doi:10.3389/fpls.2015.00547, 2015.

532 Canadell, J., Jackson, R. B., Ehleringer, J. R., Mooney, H. A., Sala, O. E. and Schulze, E.-D.: Max rooting depth of  
533 vegetation types at the global scale, *Oecologia*, 108, 583–595, doi:10.1007/s10705-016-9812-z, 1996.

534 Carvalhais, N., Forkel, M., Khomik, M., Bellarby, J., Jung, M., Migliavacca, M., Saatchi, S., Santoro, M., Thurner, M. and  
535 Weber, U.: Global covariation of carbon turnover times with climate in terrestrial ecosystems, *Nature*, 514(7521), 213–217,  
536 2014.

537 Ciemer, C., Boers, N., Hirota, M., Kurths, J., Müller-Hansen, F., Oliveira, R. S. and Winkelmann, R.: Higher resilience to  
538 climatic disturbances in tropical vegetation exposed to more variable rainfall, *Nat. Geosci.*, 12(March), doi:10.1038/s41561-  
539 019-0312-z, 2019.

540 Cosby, B. J., Hornberger, G. M., Clapp, R. B. and Ginn, T.: A statistical exploration of the relationships of soil moisture  
541 characteristics to the physical properties of soils, *Water Resour. Res.*, 20(6), 682–690, 1984.

542 Costa, M. H., Biajoli, M. C., Sanches, L., Malhado, A. C. M., Hutyrá, L. R., Da Rocha, H. R., Aguiar, R. G. and De Araújo,  
543 A. C.: Atmospheric versus vegetation controls of Amazonian tropical rain forest evapotranspiration: Are the wet and  
544 seasonally dry rain forests any different?, *J. Geophys. Res. Biogeosciences*, 115(4), 1–9, doi:10.1029/2009JG001179, 2010.

545 Dee, D. P., Uppala, S. M., Simmons, A. J., Berrisford, P., Poli, P., Kobayashi, S., Andrae, U., Balmaseda, M. A., Balsamo,  
546 G., Bauer, P., Bechtold, P., Beljaars, A. C. M., van de Berg, L., Bidlot, J., Bormann, N., Delsol, C., Dragani, R., Fuentes, M.,  
547 Geer, A. J., Haimberger, L., Healy, S. B., Hersbach, H., Hólm, E. V., Isaksen, I., Kållberg, P., Köhler, M., Matricardi, M.,  
548 McNally, A. P., Monge-Sanz, B. M., Morcrette, J. J., Park, B. K., Peubey, C., de Rosnay, P., Tavolato, C., Thépaut, J. N. and  
549 Vitart, F.: The ERA-Interim reanalysis: Configuration and performance of the data assimilation system, *Q. J. R. Meteorol.*  
550 *Soc.*, 137(656), 553–597, doi:10.1002/qj.828, 2011.

551 Ek, M. B., Mitchell, K. E., Lin, Y., Rogers, E., Grunmann, P., Koren, V., Gayno, G. and Tarpley, J. D.: Implementation of  
552 Noah land surface model advances in the National Centers for Environmental Prediction operational mesoscale Eta model, *J.*  
553 *Geophys. Res. D Atmos.*, 108(22), 1–16, doi:10.1029/2002jd003296, 2003.

554 Eshel, A. and Grünzweig, J. M.: Root-shoot allometry of tropical forest trees determined in a large-scale aeroponic system,  
555 *Ann. Bot.*, 112(2), 291–296, doi:10.1093/aob/mcs275, 2013.

556 Fan, Y., Miguez-Macho, G., Jobbágy, E. G., Jackson, R. B. and Otero-Casal, C.: Hydrologic regulation of plant rooting  
557 depth., *Proc. Natl. Acad. Sci. U. S. A.*, 114(40), 10572–10577, doi:10.1073/pnas.1712381114, 2017.

558 Fearnside, P. M.: Brazil’s Amazonian forest carbon: the key to Southern Amazonia’s significance for global climate, *Reg.*  
559 *Environ. Chang.*, 18(1), 47–61, doi:10.1007/s10113-016-1007-2, 2016.

560 Forkel, M., Carvalhais, N., Schaphoff, S., Bloh, W. V., Migliavacca, M., Thurner, M. and Thonicke, K.: Identifying  
561 environmental controls on vegetation greenness phenology through model-data integration, *Biogeosciences*, 11(23), 7025–  
562 7050, doi:10.5194/bg-11-7025-2014, 2014.

563 Guimberteau, M., Zhu, D., Maignan, F., Huang, Y., Yue, C., Dantec-Nédélec, S., Ottlé, C., Jornet-Puig, A., Bastos, A.,  
564 Laurent, P., Goll, D., Bowering, S., Chang, J., Guenet, B., Tifafi, M., Peng, S., Krinner, G., Ducharne, A., Wang, F., Wang,  
565 T., Wang, X., Wang, Y., Yin, Z., Lauerwald, R., Joetzjer, E., Qiu, C., Kim, H. and Ciais, P.: ORCHIDEE-MICT (revision  
566 4126), a land surface model for the high-latitudes: model description and validation, *Geosci. Model Dev. Discuss.*, (June), 1–  
567 65, doi:10.5194/gmd-2017-122, 2017.

568 Harris, I., Jones, P. D., Osborn, T. J. and Lister, D. H.: Updated high-resolution grids of monthly climatic observations - the  
569 CRU TS3.10 Dataset, *Int. J. Climatol.*, 34(3), 623–642, doi:10.1002/joc.3711, 2014.

570 Hijmans, R. J. and van Etten, J.: raster: Geographic data analysis and modeling, R Packag. version, 2(8), 2016.

571 Hirota, M., Holmgren, M., Van New, E. H. and Scheffer, M.: Global Resilience of Tropical Forest, *Science* (80-. ),  
572 334(October), 232–235, doi:10.1126/science.1210657, 2011.

573 Huang, S., Titus, S. J. and Wiens, D. P.: Comparison of nonlinear height–diameter functions for major Alberta tree species,  
574 *Can. J. For. Res.*, 22(9), 1297–1304, 1992.

575 Ichii, K., Hashimoto, H., White, M. A., Potter, C., Hutrya, L. R., Huete, A. R., Myneni, R. B. and Nemani, R. R.:  
576 Constraining rooting depths in tropical rainforests using satellite data and ecosystem modeling for accurate simulation of  
577 gross primary production seasonality, *Glob. Chang. Biol.*, 13(1), 67–77, doi:10.1111/j.1365-2486.2006.01277.x, 2007.

578 Jackson, R. B., Canadell, J., Ehleringer, J., Mooney, H., Sala, O. and Schulze, E.: A global analysis of root distributions for  
579 terrestrial biomes, *Oecologia*, 108, 389–411, 1996.

580 Jenik, J.: Roots and root systems in tropical trees, *Trop. trees as living Syst.*, 323, 2010.

581 Johnson, D. M., Domec, J. C., Carter Berry, Z., Schwantes, A. M., McCulloh, K. A., Woodruff, D. R., Wayne Polley, H.,  
582 Wortemann, R., Swenson, J. J., Scott Mackay, D., McDowell, N. G. and Jackson, R. B.: Co-occurring woody species have  
583 diverse hydraulic strategies and mortality rates during an extreme drought, *Plant Cell Environ.*, 41(3), 576–588,  
584 doi:10.1111/pce.13121, 2018.

585 Kattge, J., Bönisch, G., Díaz, S., Lavorel, S., Prentice, I. C., Leadley, P., Tautenhahn, S., Werner, G. D. A., Aakala, T. and  
586 Abedi, M.: TRY plant trait database–enhanced coverage and open access, *Glob. Chang. Biol.*, 2020.

587 Kelley, D. I., Prentice, I. C., Harrison, S. P., Wang, H., Simard, M., Fisher, J. B. and Willis, K. O.: A comprehensive  
588 benchmarking system for evaluating global vegetation models, *Biogeosciences*, 10(5), 3313–3340, doi:10.5194/bg-10-3313-  
589 2013, 2013.

590 Kim, H., Watanabe, E.-C., Chang, K., Yoshimura, Y., Hirabayashi, J., Famiglietti, T. and Oki, T.: Century long observation  
591 constrained global dynamic downscaling and hydrologic implication, n.d.

592 Kim, Y., Knox, R. G., Longo, M., Medvigy, D., Hutrya, L. R., Pyle, E. H., Wofsy, S. C., Bras, R. L. and Moorcroft, P. R.:  
593 Seasonal carbon dynamics and water fluxes in an Amazon rainforest, *Glob. Chang. Biol.*, 18(4), 1322–1334,  
594 doi:10.1111/j.1365-2486.2011.02629.x, 2012.

595 Kleidon, A. and Heimann, M.: A method of determining rooting depth from a terrestrial biosphere model and its impacts on  
596 the global water and carbon cycle, *Glob. Chang. Biol.*, 4(3), 275–286, doi:10.1046/j.1365-2486.1998.00152.x, 1998.

597 Kleidon, A. and Heimann, M.: Deep-rooted vegetation, Amazonian deforestation, and climate: Results from a modelling  
598 study, *Glob. Ecol. Biogeogr.*, 8(5), 397–405, doi:10.1046/j.1365-2699.1999.00150.x, 1999.

599 Kleidon, A. and Heimann, M.: Assessing the role of deep rooted vegetation in the climate system with model simulations:  
600 Mechanism, comparison to observations and implications for Amazonian deforestation, *Clim. Dyn.*, 16(2–3), 183–199,  
601 doi:10.1007/s003820050012, 2000.

602 Krysanova, V., Müller-Wohlfeil, D.-I. and Becker, A.: Development and test of a spatially distributed hydrological/water  
603 quality model for mesoscale watersheds, *Ecol. Modell.*, 106(2–3), 261–289, 1998.

604 Langan, L., Higgins, S. I. and Scheiter, S.: Climate-biomes, pedo-biomes or pyro-biomes: which world view explains the  
605 tropical forest–savanna boundary in South America?, *J. Biogeogr.*, 44(10), 2319–2330, doi:10.1111/jbi.13018, 2017.

606 Lawrence, D. M., Oleson, K. W., Flanner, M. G., Thornton, P. E., Swenson, S. C., Lawrence, P. J., Zeng, X., Yang, Z.-L.,  
607 Levis, S., Sakaguchi, K., Bonan, G. B. and Slater, A. G.: Parameterization improvements and functional and structural  
608 advances in Version 4 of the Community Land Model, *J. Adv. Model. Earth Syst.*, 3(3), 1–27, doi:10.1029/2011ms000045,  
609 2011.

610 Lee, J. E., Oliveira, R. S., Dawson, T. E. and Fung, I.: Root functioning modifies seasonal climate, *Proc. Natl. Acad. Sci. U.*  
611 *S. A.*, 102(49), 17576–17581, doi:10.1073/pnas.0508785102, 2005.

612 Leuschner, C., Moser, G., Bertsch, C., Röderstein, M. and Hertel, D.: Large altitudinal increase in tree root/shoot ratio in  
613 tropical mountain forests of Ecuador, *Basic Appl. Ecol.*, 8(3), 219–230, 2007.

614 Lewis, S. L., Brando, P. M., Phillips, O. L., Van Der Heijden, G. M. F. and Nepstad, D.: The 2010 Amazon drought, *Science*  
615 (80- ), 331(6017), 554, doi:10.1126/science.1200807, 2011.

616 Li, W., Houghton, R. A., Bontemps, S., MacBean, N., Lamarche, C., Ciais, P., Peng, S. and Defourny, P.: Gross and net land  
617 cover changes in the main plant functional types derived from the annual ESA CCI land cover maps (1992–2015), *Earth*  
618 *Syst. Sci. Data*, 10(1), 219–234, doi:10.5194/essd-10-219-2018, 2018.

619 Liu, Y. Y., Dorigo, W. A., Parinussa, R. M., De Jeu, R. A. M., Wagner, W., McCabe, M. F., Evans, J. P. and Van Dijk, A. I.  
620 J. M.: Trend-preserving blending of passive and active microwave soil moisture retrievals, *Remote Sens. Environ.*,  
621 123(October 2006), 280–297, doi:10.1016/j.rse.2012.03.014, 2012.

622 Liu, Y. Y., van Dijk, A. I. J. M., McCabe, M. F., Evans, J. P. and de Jeu, R. A. M.: Global vegetation biomass change (1988-  
623 2008) and attribution to environmental and human drivers, *Glob. Ecol. Biogeogr.*, 22(6), 692–705, doi:10.1111/geb.12024,  
624 2013.

625 Malhi, Y., Aragao, L. E. O. C., Galbraith, D., Huntingford, C., Fisher, R., Zelazowski, P., Sitch, S., McSweeney, C. and  
626 Meir, P.: Exploring the likelihood and mechanism of a climate-change-induced dieback of the Amazon rainforest, *Proc. Natl.*  
627 *Acad. Sci.*, 106(49), 20610–20615, doi:10.1073/pnas.0804619106, 2009.

628 Markewitz, D., Devine, S., Davidson, E. A., Brando, P. and Nepstad, D. C.: Soil moisture depletion under simulated drought  
629 in the Amazon: Impacts on deep root uptake, *New Phytol.*, 187(3), 592–607, doi:10.1111/j.1469-8137.2010.03391.x, 2010.

630 Martens, B., Miralles, D. G., Lievens, H., Van Der Schalie, R., De Jeu, R. A. M., Fernández-Prieto, D., Beck, H. E., Dorigo,  
631 W. A. and Verhoest, N. E. C.: GLEAM v3: Satellite-based land evaporation and root-zone soil moisture, *Geosci. Model*  
632 *Dev.*, 10(5), 1903–1925, doi:10.5194/gmd-10-1903-2017, 2017.

633 Masson, V., Champeaux, J. L., Chauvin, F., Meriguet, C. and Lacaze, R.: A global database of land surface parameters at 1-  
634 km resolution in meteorological and climate models, *J. Clim.*, 16(9), 1261–1282, doi:10.1175/1520-0442-16.9.1261, 2003.

635 Miralles, D. G., Holmes, T. R. H., De Jeu, R. A. M., Gash, J. H., Meesters, A. G. C. A. and Dolman, A. J.: Global land-  
636 surface evaporation estimated from satellite-based observations, *Hydrol. Earth Syst. Sci.*, 15(2), 453–469, doi:10.5194/hess-  
637 15-453-2011, 2011.

638 Mokany, K., Raison, R. J. and Prokushkin, A. S.: Critical analysis of root: Shoot ratios in terrestrial biomes, *Glob. Chang.*  
639 *Biol.*, 12(1), 84–96, doi:10.1111/j.1365-2486.2005.001043.x, 2006.

640 Nachtergaele, F. van, Velthuisen, H., Verelst, L., Batjes, N., Dijkshoorn, K. van Engelen, V., Fischer, G., Jones, A.,  
641 Montanarella, L. and Petri, M.: Harmonized world soil database, Food and Agriculture Organization of the United Nations,  
642 [online] Available from: [http://www.fao.org/soils-portal/soil-survey/soil-maps-and-databases/harmonized-world-soil-](http://www.fao.org/soils-portal/soil-survey/soil-maps-and-databases/harmonized-world-soil-database-v12/en/)  
643 [database-v12/en/](http://www.fao.org/soils-portal/soil-survey/soil-maps-and-databases/harmonized-world-soil-database-v12/en/), 2009.

644 Nemani, R. R., Keeling, C. D., Hashimoto, H., Jolly, W. M., Piper, S. C., Tucker, C. J., Myneni, R. B. and Running, S. W.:  
645 Climate-driven increases in global terrestrial net primary production from 1982 to 1999, *Science (80- )*, 300(5625), 1560–  
646 1563, doi:10.1126/science.1082750, 2003.

647 New, M., Hulme, M. and Jones, P.: Representing twentieth century space-time climate variability. Part II: development of a  
648 1901-1996 monthly grids of terrestrial surface climate, *J. Clim.*, 13, 2217–2238, 2000.

649 Nikolova, P. S., Zang, C. and Pretzsch, H.: Combining tree-ring analyses on stems and coarse roots to study the growth  
650 dynamics of forest trees: A case study on Norway spruce (*Picea abies* [L.] H. Karst), *Trees - Struct. Funct.*, 25(5), 859–872,  
651 doi:10.1007/s00468-011-0561-y, 2011.

652 Ostle, N. J., Smith, P., Fisher, R., Ian Woodward, F., Fisher, J. B., Smith, J. U., Galbraith, D., Levy, P., Meir, P., McNamara,  
653 N. P. and Bardgett, R. D.: Integrating plant-soil interactions into global carbon cycle models, *J. Ecol.*, 97(5), 851–863,  
654 doi:10.1111/j.1365-2745.2009.01547.x, 2009.

655 Pelletier, J. D., Broxton, P. D., Hazenberg, P., Zeng, X., Troch, P. A., Niu, G.-Y., Williams, Z., Brunke, M. A. and Gochis,  
656 D.: A gridded global data set of soil, intact regolith, and sedimentary deposit thicknesses for regional and global land surface  
657 modeling, *J. Adv. Model. Earth Syst.*, 8, 41–65, doi:10.1002/2017MS001065, 2016.

658 Poorter, H., Niklas, K. J., Reich, P. B., Oleksyn, J., Poot, P. and Mommer, L.: Biomass allocation to leaves, stems and roots:



659 meta-analyses of interspecific variation and environmental control, *New Phytol.*, 193(1), 30–50, 2012.

660 Prentice, I. C., Sykes, M. T. and Cramer, W.: A simulation model for the transient effects of climate change on forest  
661 landscapes, *Ecol. Modell.*, 65(1–2), 51–70, 1993.

662 R Core Team: R: A language and environment for statistical computing. R Foundatoin for Statistical Computing, [online]  
663 Available from: <https://www.r-project.org/>, 2019.

664 Rodell, M., Houser, P. R., Jambor, U., Gottschalck, J., Mitchell, K., Meng, C.-J., Arsenault, K., Cosgrove, B., Radakovich,  
665 J., Bosilovich, M., Entin, J. K., Walker, J. P., Lohmann, D. and Toll, D.: The Global Land Data Assimilation System, *Bull.*  
666 *Am. Meteorol. Soc.*, 85(March), 381–394, 2004.

667 Saatchi, S. S., Harris, N. L., Brown, S., Lefsky, M., Mitchard, E. T. A., Salas, W., Zutta, B. R., Buermann, W., Lewis, S. L.,  
668 Hagen, S., Petrova, S., White, L., Silman, M. and Morel, A.: Benchmark map of forest carbon stocks in tropical regions  
669 across three continents, *Proc. Natl. Acad. Sci.*, 108(24), 9899–9904, doi:10.1073/pnas.1019576108, 2011.

670 Sakschewski, B., von Bloh, W., Drüke, M., Sörensson, A. A., Ruscica, R., Langerwisch, F., Billing, M., Bereswill, S.,  
671 Hirota, M., Oliveira, R. S., Heinke, J. and Thonicke, K.: LPJmL4.0-VR Model Code. Zenodo Data Services,  
672 doi:<https://doi.org/10.5281/zenodo.4709250>, 2021a.

673 Sakschewski, B., von Bloh, W., Drüke, M., Sörensson, A. A., Ruscica, R., Langerwisch, F., Billing, M., Bereswill, S.,  
674 Hirota, M., Oliveira, R. S., Heinke, J. and Thonicke, K.: LPJmL4.0-VR Model Output. Zenodo data services,  
675 doi:<https://doi.org/10.5281/zenodo.4709166>, 2021b.

676 Saleska, S. R., Da Rocha, H. R., Huete, A. R., Nobre, A. D., Artaxo, P. E. and Shimabukuro, Y. E.: LBA-ECO CD-32 Flux  
677 Tower Network Data Compilation, Brazilian Amazon: 1999-2006, , doi:10.3334/ORNLDAAC/1174, 2013.

678 Schaphoff, S., von Bloh, W., Rammig, A., Thonicke, K., Biemans, H., Forkel, M., Gerten, D., Heinke, J., Jägermeyr, J.,  
679 Knauer, J., Langerwisch, F., Lucht, W., Müller, C., Rolinski, S. and Waha, K.: LPJmL4 – a dynamic global vegetation  
680 model with managed land – Part 1: Model description, *Geosci. Model Dev.*, 11(4), 1343–1375, doi:10.5194/gmd-11-1343-  
681 2018, 2018a.

682 Schaphoff, S., von Bloh, W., Thonicke, K., Biemans, H., M, F., Heinke, J., Jägermyer, J., Müller, C., Rolinski, S., Waha, K.,  
683 Stehfest, E., de Waal, L., Heyder, U., Gumpenberger, M. and Beringer, T.: LPJmL4 Model Code, V. 4.0. GFZ Data  
684 Services, , doi:<https://doi.org/10.5880/pik.2018.002>, 2018b.

685 Schymanski, S. J., Sivapalan, M., Roderick, M. L., Beringer, J. and Hutley, L. B.: An optimality-based model of the coupled  
686 soil moisture and root dynamics, *Hydrol. Earth Syst. Sci.*, 12(3), 913–932, doi:10.5194/hess-12-913-2008, 2008.

687 Sheffield, J., Goteti, G. and Wood, E. F.: Development of a 50-year high-resolution global dataset of meteorological forcings  
688 for land surface modeling, *J. Clim.*, 19(13), 3088–3111, doi:10.1175/JCLI3790.1, 2006.

689 Shinozaki, K., Yoda, K. and Kira, T.: A quantitative analysis of plant form - The pipe model theory, *Japanese J. Ecol.*, 14(3),  
690 1964.

691 Smith, B., Wärlind, D., Arneth, A., Hickler, T., Leadley, P., Siltberg, J. and Zaehle, S.: Implications of incorporating N  
692 cycling and N limitations on primary production in an individual-based dynamic vegetation model, *Biogeosciences*, 11(7),  
693 2027–2054, doi:10.5194/bg-11-2027-2014, 2014.

694 Sörensson, A. A. and Ruscica, R. C.: Intercomparison and Uncertainty Assessment of Nine Evapotranspiration Estimates  
695 Over South America, *Water Resour. Res.*, 54(4), 2891–2908, doi:10.1002/2017WR021682, 2018.

696 Staal, A., Tuinenburg, O. A., Bosmans, J. H. C., Holmgren, M., Van Nes, E. H., Scheffer, M., Zemp, D. C. and Dekker, S.  
697 C.: Forest-rainfall cascades buffer against drought across the Amazon, *Nat. Clim. Chang.*, 8(6), 539–543,  
698 doi:10.1038/s41558-018-0177-y, 2018.

699 Staver, A. C., Archibald, S. and Levin, S. A.: The global extent and determinants of savanna and forest as alternative biome  
700 states, *Science (80-. )*, 334(6053), 230–232, doi:10.1126/science.1210465, 2011.

701 Tans, P. and Keeling, R.: Trends in Atmospheric Carbon Dioxide, *Natl. Ocean. Atmos. Adm. Earth Syst. Res. Lab.* [online]

702 Available from: <http://www.esrl.noaa.gov/gmd/ccgg/trends>, 2015.

703 Thonicke, K., Venevsky, S., Sitch, S. and Cramer, W.: The role of fire disturbance for global vegetation dynamics: Coupling  
704 fire into a dynamic global vegetation model, *Glob. Ecol. Biogeogr.*, 10(6), 661–677, doi:10.1046/j.1466-822X.2001.00175.x,  
705 2001.

706 Waring, R. H., Schroeder, P. E. and Oren, R.: Application of the pipe model theory to predict canopy leaf area, *Can. J. For.*  
707 *Res.*, 12(3), 556–560, doi:<https://doi.org/10.1139/x82-086>, 1982.

708 Warren, J. M., Hanson, P. J., Iversen, C. M., Kumar, J., Walker, A. P. and Wullschleger, S. D.: Root structural and  
709 functional dynamics in terrestrial biosphere models - evaluation and recommendations, *New Phytol.*, 205(1), 59–78,  
710 doi:10.1111/nph.13034, 2015a.

711 Warren, J. M., Hanson, P. J., Iversen, C. M., Kumar, J., Walker, A. P. and Wullschleger, S. D.: Root structural and  
712 functional dynamics in terrestrial biosphere models - evaluation and recommendations, *New Phytol.*, 205(1), 59–78,  
713 doi:10.1111/nph.13034, 2015b.

714 Weedon, G. P., Gomes, S., Viterbo, P., Shuttleworth, W. J., Blyth, E., Österle, H., Adam, J. C., Bellouin, N., Boucher, O.  
715 and Best, M.: Creation of the WATCH Forcing Data and Its Use to Assess Global and Regional Reference Crop Evaporation  
716 over Land during the Twentieth Century, *J. Hydrometeorol.*, 12(5), 823–848, doi:10.1175/2011jhm1369.1, 2011.

717 Weedon, G. P., Balsamo, G., Bellouin, N., Gomes, S., Best, M. J. and Viterbo, P.: Data methodology applied to ERA-  
718 Interim reanalysis data, *Water Resour. Res.*, 50, 7505–7514, doi:10.1002/2014WR015638.Received, 2014.

719 Wu, J., Albert, L. P., Lopes, A. P., Restrepo-Coupe, N., Hayek, M., Wiedemann, K. T., Guan, K., Stark, S. C.,  
720 Christoffersen, B., Prohaska, N., Tavares, J. V., Marostica, S., Kobayashi, H., Ferreira, M. L., Campos, K. S., Dda Silva, R.,  
721 Brando, P. M., Dye, D. G., Huxman, T. E., Huete, A. R., Nelson, B. W. and Saleska, S. R.: Leaf development and  
722 demography explain photosynthetic seasonality in Amazon evergreen forests, *Science* (80-. ), 351(6276), 972–976,  
723 doi:10.1126/science.aad5068, 2016.

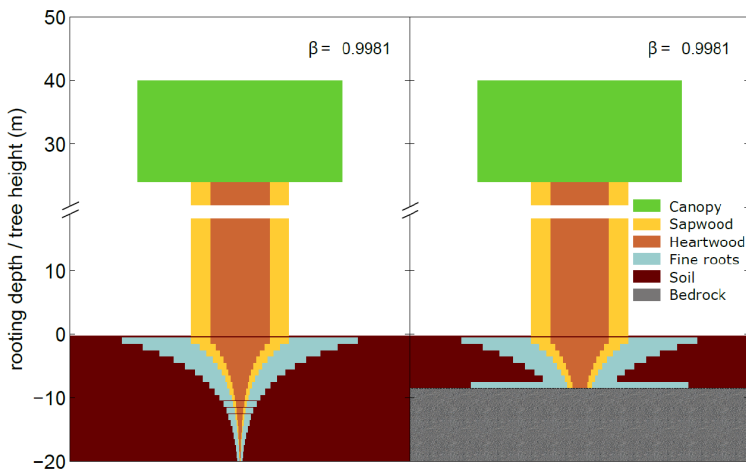
724 Wuyts, B., Champneys, A. R. and House, J. I.: Amazonian forest-savanna bistability and human impact, *Nat. Commun.*,  
725 8(May), 1–11, doi:10.1038/ncomms15519, 2017.

726 Xiao, C. W., Yuste, J. C., Janssens, I. A., Roskams, P., Nachtergale, L., Carrara, A., Sanchez, B. Y. and Ceulemans, R.:  
727 Above- and belowground biomass and net primary production in a 73-year-old Scots pine forest, *Tree Physiol.*, 23(8), 505–  
728 516, doi:10.1093/treephys/23.8.505, 2003.

729 Xiao, X., Hagen, S., Zhang, Q., Keller, M. and Moore, B.: Detecting leaf phenology of seasonally moist tropical forests in  
730 South America with multi-temporal MODIS images, *Remote Sens. Environ.*, 103(4), 465–473,  
731 doi:10.1016/j.rse.2006.04.013, 2006.

732 Zemp, D. C., Schleussner, C. F., Barbosa, H. M. J., Hirota, M., Montade, V., Sampaio, G., Staal, A., Wang-Erlandsson, L.  
733 and Rammig, A.: Self-amplified Amazon forest loss due to vegetation-atmosphere feedbacks, *Nat. Commun.*, 8, 1–10,  
734 doi:10.1038/ncomms14681, 2017.

735



736

737

738

739

740

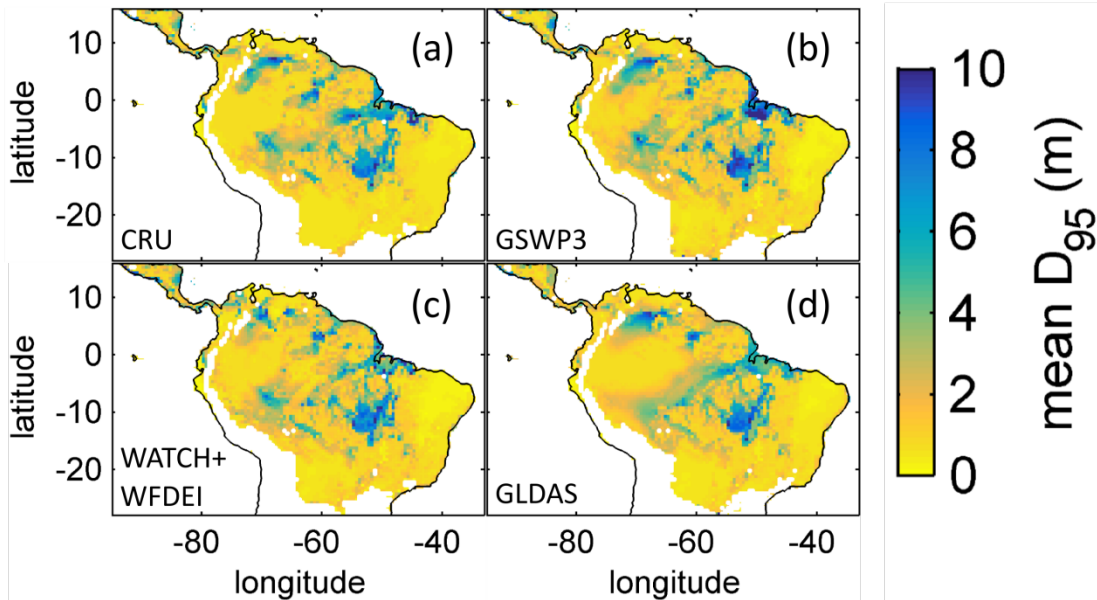
741

742

743

744

Figure 1: Visualization of belowground carbon allocation to different carbon pools of a tree PFT in LPJmL4.0-VR with a height of 40m and a  $D_{95\_max}$  of 14m (sub-PFT no. 8 in Table A2) growing in a grid cell with a soil depth of 20m (left panel) and a soil depth of 7m (right panel). As for stem sapwood, also root sapwood needs to satisfy the pipe model. In the first soil layer root sapwood cross-sectional area is equal to stem sapwood cross-sectional area, as all water taken up by fine roots needs to pass this layer. In each following soil layer the root sapwood cross-sectional area is reduced by the sum of the relative amount of fine roots of all soil layers above, thus adjusting the amount of sapwood needed to satisfy the pipe model. Please also see Supplementary Video 1 for a visualization of root growth and development of belowground carbon pools over time under [http://www.pik-potsdam.de/~borissa/LPJmL4\\_VR/Supplementary\\_Video\\_1.pptx](http://www.pik-potsdam.de/~borissa/LPJmL4_VR/Supplementary_Video_1.pptx).



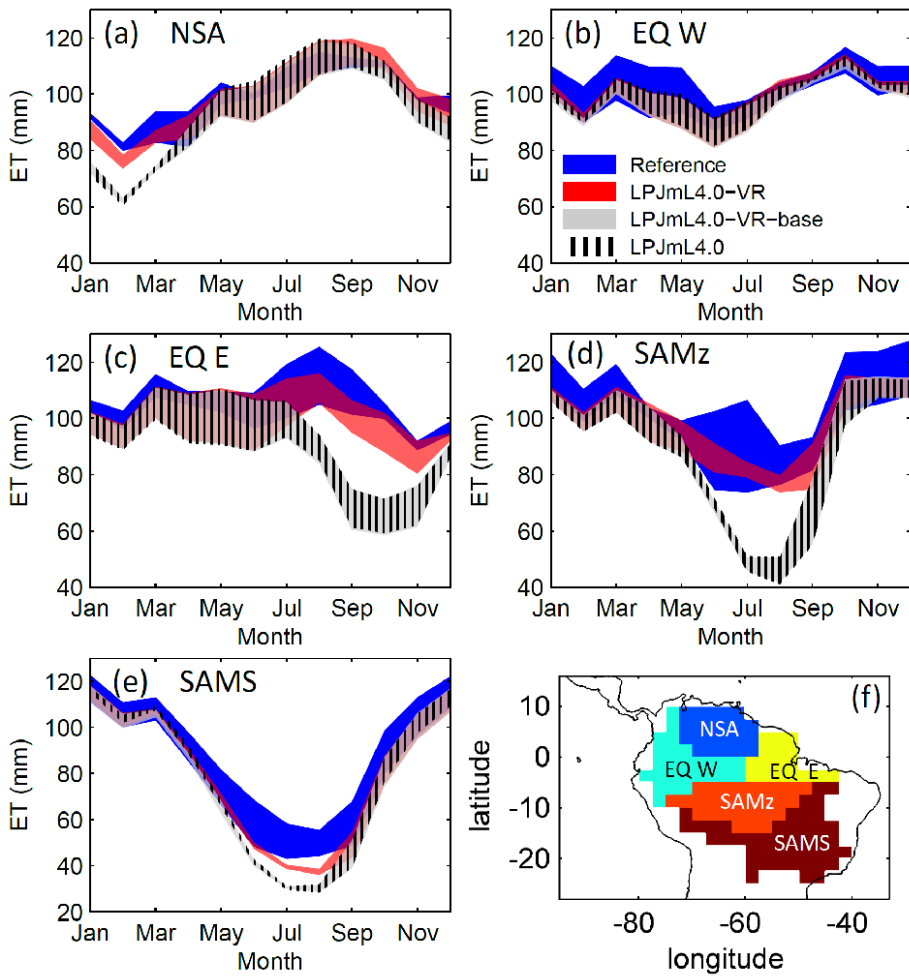
745

746

747

748

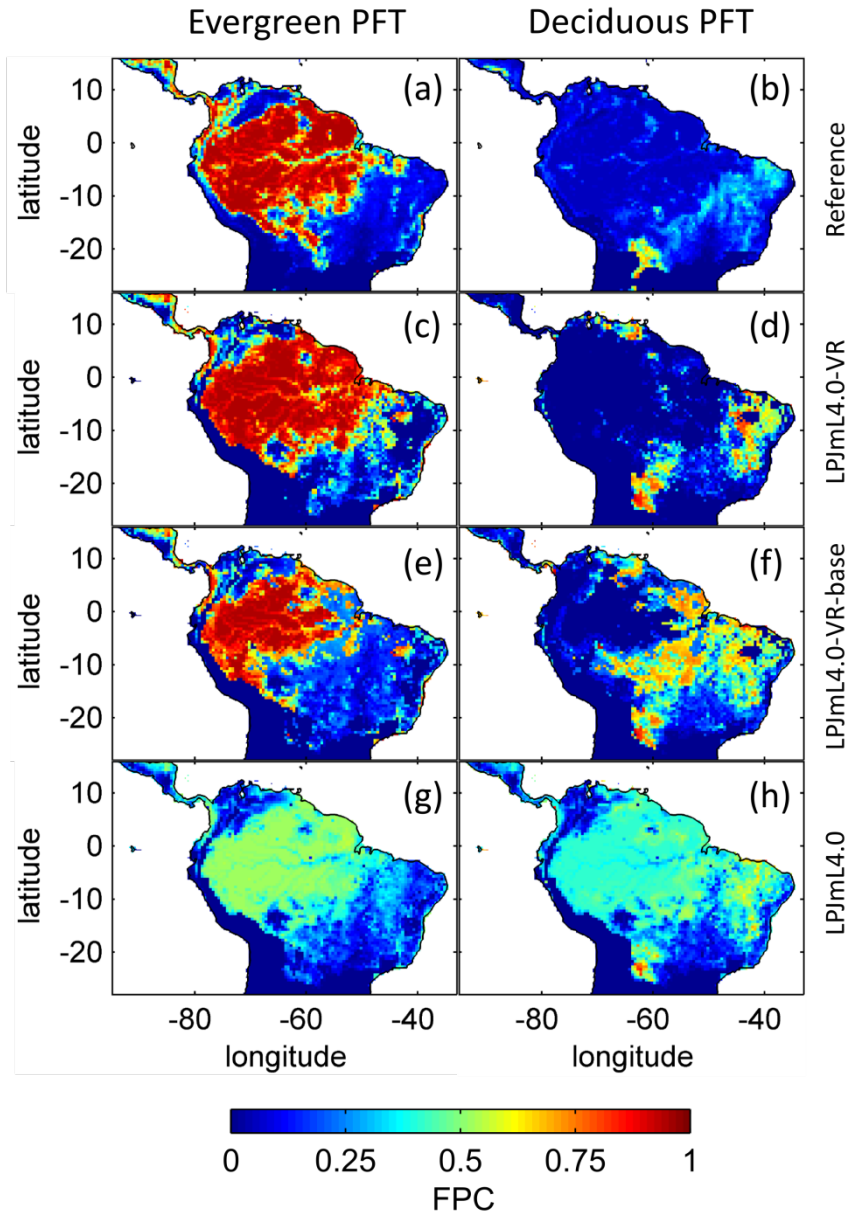
Figure 2: Regional NPP-weighted mean rooting depth ( $\overline{D_{95}}$ ) of all sub-PFTs (evergreen and deciduous PFTs combined) for 2001-2010 and different climate inputs simulated with LPJmL4.0-VR. a) CRU climate input. b) GSWP3 climate input. c) WATCH+WFDEI climate input. d) GLDAS climate input. The color scale maximum is set to 10 m.



749

750  
751  
752  
753  
754

**Figure 3: Comparisons of continental scale gridded ET products against simulated ET within 5 regional climatological clusters (a-e) as defined in Sect. 2.5.1. Shown is the mean annual cycle of 1981-2010 and the mean for the whole cluster area. Corridors denote the minimum-maximum range between either the “Reference” ET products (Sect. 2.5.1 Validation data) or the model outputs under the different climate forcings used in this study. f) Geographical extent of climatological clusters (adapted from Sörensson and Ruscica, 2018). Statistical measures of the individual comparisons can be found in Table B3 (comparisons of corridor means).**



755  
756  
757  
758  
759  
760

**Fig. 4: Foliage projected cover (FPC) of evergreen (a, c, e, g) and deciduous (b, d, f, h) PFTs over the study region. a)-b) Satellite-derived vegetation composition from ESA Land cover CCI V2.0.7 (Li et al., 2018) reclassified to the PFTs of LPJmL as in (Forkel et al., 2014). b)-c) LPJmL4.0-VR. d)-e) LPJmL4.0-VR-base. f)-g) LPJmL4.0. All LPJmL model versions were forced with CRU climate input. The shown FPC for all models refers to 2001-2010. For statistical measures of individual comparisons between model versions (c-h) and satellite derived vegetation composition (a-b) see Table B4.**

761 **Appendix A**

762 **1 Methods**

763 **A new tree rooting scheme for LPJmL4.0**

764 In this section we describe the new basic scheme for soil layer partitioning, the new tree rooting scheme, the simulation of  
765 belowground carbon investment, and how different tree rooting strategies (implemented in the new scheme) compete.

766 **1.1 Scheme for soil layer partitioning**

767 LPJmL4.0 employs a globally universal soil depth of 3 m. For LPJmL4.0-VR we extended the general maximum soil depth  
768 to 20 m (but restrict it to local soil depth information at spatial model resolution; Manuscript Sect. 2.3.2). We applied the  
769 same basic scheme for soil layer partitioning from LPJmL4.0 (Schaphoff et al., 2018a), in order to keep model differences

770 small (Table A1). We chose a maximum of 20 m soil depth to considerably increase the maximum soil depth compared to  
 771 constant 3 m in LPJmL4.0, while keeping the increment of computational demand connected to adding more soil layers  
 772 within an acceptable range. Equal to LPJmL4.0 (Schaphoff et al., 2018a), we use a grid cell specific soil texture information  
 773 which is applied to the whole soil column.

### 774 1.2 Water balance, infiltration and percolation

775 We here provide a very brief description of LPJmL's water balance and soil hydrology. A detailed description can be found  
 776 in Schaphoff et al. (2018).

777 Hydraulic conductivity and water holding capacity (water content at permanent wilting point, at field capacity, and at  
 778 saturation) for each grid cell are derived from information on soil texture from the Harmonized World Soil Database  
 779 (HWSD) version 1 (Nachtergaele et al., 2009) and relationships between texture and hydraulic properties from Cosby et al.  
 780 (1984). Each soil layer's (Appendix A Sect. 1.1) water content can be altered by infiltrating rainfall and percolation. The soil  
 781 water content of the first soil layer determines the infiltration rate of rain and irrigation water. The excess water that does not  
 782 infiltrate generates surface water runoff. Water percolation through the soil layers is calculated by the storage routine  
 783 technique (Arnold et al., 1990) as used in regional hydrological models such as SWIM (Krysanova et al., 1998). Water  
 784 percolation thus depends on the hydraulic conductivity of each soil layer and the soil water content between field capacity  
 785 and saturation at the beginning and the end of the day for all soil layers. Similar to water infiltration into the first soil layer,  
 786 percolation in each soil layer is limited by the soil moisture of the following lower layer. Excess water over the saturation  
 787 levels forms lateral runoff in each layer and contributes to subsurface runoff. Surface and subsurface runoff accumulate to  
 788 river discharge. The routines for water balance, infiltration and percolation were not changed for LPJmL4.0-VR. Thus the  
 789 routines now apply for soil columns of up to 20 m depth (Appendix A Sect. 1.1).

### 790 1.3 Diversifying general tree rooting strategies

791 In LPJmL4.0 the tree rooting strategy of a PFT is reflected by a certain prescribed vertical distribution of fine roots  
 792 throughout the soil column. Each soil layer  $l$  is assigned a PFT specific relative amount of fine roots  $rootdist_l$ :

$$793 \quad rootdist_l = rootdist(z_l) - rootdist(z_{l-1}) \quad \text{Eq. (A1)}$$

794 where  $z_l$  is the soil layer boundary depth in cm of each soil layer  $l$  and  $rootdist(z_l)$  is the relative amount of fine roots between  
 795 the forest floor and the boundary of soil layer  $l$ . The function  $rootdist(z)$  is defined following Jackson *et al.* (1996):

$$796 \quad rootdist(z) = \frac{1 - \beta^z}{1 - \beta^{z_{bottom}}} \quad \text{Eq. (A2)}$$

797 where  $\beta$  is a constant parameter shaping the vertical distribution of fine roots and therefore determining the tree rooting  
 798 strategy and  $z_{bottom}$  is the maximum soil depth in cm. In LPJmL4.0 each PFT is assigned a different  $\beta$ -value reflecting the  
 799 average tree rooting strategy on this broad PFT scale (Schaphoff et al., 2018a).

800 To quantify the maximum rooting depth of PFTs that actually results from this approach (Eq. A1&A2) we here calculate the  
 801 depth at which the cumulated fine root biomass from the soil surface downwards is 95% ( $D_{95\_max}$ ) as follows:

$$802 \quad D_{95\_max} = \frac{\log(1 - 0.95 \cdot (1 - \beta^{z_{bottom}}))}{\log(\beta)} \quad \text{Eq. (A3)}$$

803 In LPJmL4.0 the  $\beta$ -values of tropical tree PFTs are set to 0.962 for the tropical broadleaved evergreen tree and to 0.961 for  
 804 the tropical broadleaved deciduous tree following Jackson et al. (1996). According to Eq. A3 both PFTs have a  $D_{95\_max}$   
 805 smaller than 1 m. For LPJmL4.0-VR we extended this representation of tree rooting strategies by splitting both tropical tree  
 806 PFTs into 10 sub-PFTs and assigned each with a different  $\beta$ -value. These values were chosen to cover a range of different  
 807  $D_{95\_max}$  values between 0.5 and 18m (Table A2). We chose 18 m as the largest  $D_{95\_max}$  value in order to avoid that roots of the  
 808 respective sub-PFT significantly exceed the maximum soil depth of 20 m (see also Appendix A Sect. 1.5). Fig. A1 shows the  
 809 new maximum distribution of fine roots throughout the soil column for the different  $\beta$ -values chosen (Table A2).

## 810 1.4 Belowground carbon investment

811 Tropical trees can avoid water stress under seasonally dry climate by growing relatively deep roots (Brum et al., 2019; Fan et  
812 al., 2017) which goes along with increased below-ground carbon investment. Thus, the need for deep water access creates a  
813 trade-off between below-ground and above-ground carbon investment. Therefore, a new carbon allocation scheme for  
814 LPJmL4.0-VR was necessary to account for this trade-off in order to reproduce observed local to regional patterns and  
815 distributions of tree rooting strategies instead of prescribing them. In LPJmL4.0-VR we introduced two new carbon pools,  
816 namely root sapwood and root heartwood. Like stem sapwood in LPJmL4.0, also root sapwood in LPJmL4.0-VR needs to  
817 satisfy the assumptions of the pipe model (Shinozaki et al., 1964; Waring et al., 1982). The pipe model describes, that for a  
818 certain amount of leaf area a certain amount of water conducting tissue must be available. In LPJmL4.0 the cross-sectional  
819 area of stem sapwood needs to be proportional to the leaf area  $LA_{ind}$  as follows:

$$820 LA_{ind} = k_{la:sa} \cdot SA_{ind} \quad \text{Eq. (A4)}$$

821 where  $k_{la:sa}$  is a constant describing the ratio of leaf area and stem sapwood cross-sectional area ( $SA_{ind}$ ). In LPJmL4.0-VR we  
822 also apply the pipe model to root sapwood. Root sapwood cross-sectional area in the first soil layer is equal to stem sapwood  
823 cross-sectional area, as all water must be transported through the root sapwood within this soil layer. In the following soil  
824 layers downwards, root sapwood cross-sectional area decreases by the relative amount of fine roots in all soil layers above  
825 (Fig. 1). Root sapwood is turned into root heartwood at an equal rate as stem sapwood is turned into stem heartwood, i.e. 5%  
826 per year as implemented in LPJmL4.0 (see Schaphoff *et al.*, 2018).

## 827 1.5 Root growth

828 In LPJmL4.0 (Schaphoff et al., 2018a) no vertical root growth is simulated, thus the relative distribution of fine roots over  
829 the soil column is constant over space and time. It means that PFTs starting from bare ground in a sapling stage display the  
830 same relative distribution of fine roots throughout the soil column as a full-grown forest which contradicts the principles of  
831 dynamic root growth over a tree's lifetime. Applied to LPJmL4.0-VR, the belowground biomass of an initialized deep  
832 rooting-strategy sub-PFT would exceed its aboveground biomass (AGB) by order of magnitudes when considering coarse  
833 roots. Consequently, deep rooting strategies would always be disadvantageous, calling for modelling gradual root growth in  
834 LPJmL4.0-VR. Unfortunately, little is known about how roots of tropical trees grow over time, given the fact that this  
835 research field is strongly time and resource demanding, and at the same time the variety of tree species, rooting strategies  
836 and environmental conditions are large (Jenik, 2010). A recent promising study by Brum *et al.* (2019) was able to capture the  
837 effective functional rooting depth (EFRD) of different size classes of 12 dominant tree species in a seasonal Amazon forest  
838 where tree roots grow considerably deep with maximum values reaching below 30 m. To our knowledge this is the only  
839 study capturing the relation between the size of tropical trees and their maximum rooting depth in a high spatial resolution  
840 covering sufficient tree-height classes in order to derive a functional relation between tree height and rooting depth.  
841 Following the findings of Brum *et al.* (2019), we here implemented a logistic root growth function, which calculates a  
842 general maximum conceivable tree rooting depth  $D$  depending on tree height:

$$843 D = \frac{S}{1 + e^{-kSh} \cdot \left(\frac{S}{D_0} - 1\right)} \quad \text{Eq. (A5)}$$

844 where  $S$  is the maximum soil depth in the model (20 m),  $k$  is a dimensionless constant defining the growth rate of the  
845 standard logistic growth function (set to 0.02),  $h$  is the average tree height of a PFT in m and  $D_0$  is the initial rooting depth of  
846 tree PFT saplings (set to 0.1 m; tree saplings in LPJmL4.0-VR are initialized with a height of 0.45 m as in LPJmL4.0). The  
847 distribution of fine root biomass of each sub-PFT in the soil column is then adjusted according to  $D$  at each time step, by  
848 restricting  $z_{bottom}$  in Eq. A2. Every time  $D$  crosses a specific soil layer boundary (Appendix A Sect. 1.1)  $z_{bottom}$  is assigned the  
849 value of the next soil layer boundary. Thus,  $z_{bottom}$  increases in discrete steps. Consequently, each tree rooting strategy  
850 allowed for in this study (Appendix A Sect. 1.3) shows a logistic growth of rooting depth which is dependent on the sub-PFT

851 height and which saturates towards its specific maximum rooting depth (Fig. A2). Therefore, limitations of aboveground  
 852 sub-PFT growth due to below-ground carbon investment of different tree rooting strategies (Appendix A Sect. 1.4) are equal  
 853 in the sapling phase of all sub-PFTs (starting from bare ground) and start to diverge with increasing sub-PFT height. In the  
 854 case  $D$  exceeds the grid cell specific local soil depth (as prescribed by the soil thickness input, see Manuscript Sect. 2.3.2) all  
 855 the respective fine root biomass exceeding this soil depth is transferred to the last soil layer matching this soil depth (see also  
 856 Fig. 1 right panel and Supplementary Video 1 for a visualization of root growth under [http://www.pik-](http://www.pik-potsdam.de/~borissa/LPJmL4_VR/Supplementary_Video_1.pptx)  
 857 [potsdam.de/~borissa/LPJmL4\\_VR/Supplementary\\_Video\\_1.pptx](http://www.pik-potsdam.de/~borissa/LPJmL4_VR/Supplementary_Video_1.pptx)).

858 The parameter  $k$  in Eq. A5 was chosen to preserve the slope of the 75%ile function describing the relation between tree  
 859 height and EFRD as found in Brum *et al.* (2019). We could not implement any of the original functions as suggested in  
 860 Brum *et al.* (2019) since they deliver unrealistic low values of rooting depth (between 0 and 10cm) for trees  $\leq 10$  m, which  
 861 results in a strong competitive disadvantage against herbaceous PFTs in LPJmL4.0-VR. We decided for the slope of the  
 862 75%ile function to allow for root growth rates close to the maximum which also allows for the largest  $D_{95\_max}$  values in this  
 863 study (Appendix A Sect. 1.3) to be reached. Note that Brum *et al.* (2019) originally propose a relation between tree diameter  
 864 at breast height ( $DBH$ ) and EFRD. For our purposes we related rooting depth to tree height ( $h$ ), which is calculated from  
 865  $DBH$  in in LPJmL4.0 according to Huang *et al.* (1992):

$$866 \quad h = k_{allom2} \cdot DBH^{k_{allom3}} \quad \text{Eq. (A6)}$$

867 where  $k_{allom2}$  and  $k_{allom3}$  are constants set to 40 and 0.67, respectively (Schaphoff *et al.*, 2018a).

## 868 1.6 Competition of rooting strategies

869 In each grid-cell all sub-PFTs of the evergreen and deciduous tree PFTs compete for light and water following LPJmL4.0's  
 870 approach to simulate plant competition. In LPJmL4.0, the number of new PFT saplings per unit area ( $est_{PFT}$  in  $\text{ind m}^{-2} \text{a}^{-1}$ )  
 871 which are established each year is proportional to a maximum establishment rate  $k_{est}$  and to the sum of foliage projected  
 872 cover (FPC; a relative number between 0 and 1) of all tree PFTs present in a grid cell ( $FPC_{TREE}$ ). It declines in proportion to  
 873 canopy light attenuation when the sum of woody FPCs exceeds 0.95, thus simulating a decline in establishment success with  
 874 canopy closure (Prentice *et al.*, 1993):

$$875 \quad est_{PFT} = k_{est} \cdot (1 - e^{(-5 \cdot (1 - FPC_{TREE}))}) \cdot \frac{1 - FPC_{TREE}}{n_{estTREE}} \quad \text{Eq. (A7)}$$

876 where  $n_{estTREE}$  is the number of established tree individuals ( $\text{ind m}^{-2} \text{a}^{-1}$ ). It is important to note that LPJmL4.0 does not  
 877 simulate individual trees. As a common method of DGVM's, tree saplings enter the average individual of a PFT as described  
 878 in Schaphoff *et al.* (2018).

879 To allow for environmental filtering of tree rooting strategies which are best adapted to local environmental conditions, we  
 880 changed the standard tree establishment scheme in LPJmL4.0-VR. Now, the establishment rates of sub-PFTs ( $est_{sub\_PFT}$ ) are  
 881 additionally weighted by the local dominance of each sub-PFT as follows:

$$882 \quad est_{sub\_PFT} = k_{est} \cdot (1 - e^{(-5 \cdot (1 - FPC_{TREE}))}) \cdot \frac{1 - FPC_{TREE}}{n_{estTREE}} \cdot \frac{FPC_{sub\_PFT}}{FPC_{TREE}} \cdot n_{estTREE} \quad \text{Eq. (A8)}$$

883 where  $FPC_{sub\_PFT}$  is the FPC of each sub-PFT. The new term leads to a higher establishment rate for productive sub-PFTs  
 884 relative to their spatial dominance and vice versa, without changing the overall establishment rate as set by Prentice *et al.*  
 885 (1993). This function has the effect that non-viable sub-PFTs are outcompeted over time.

## 886 1.7 Background mortality

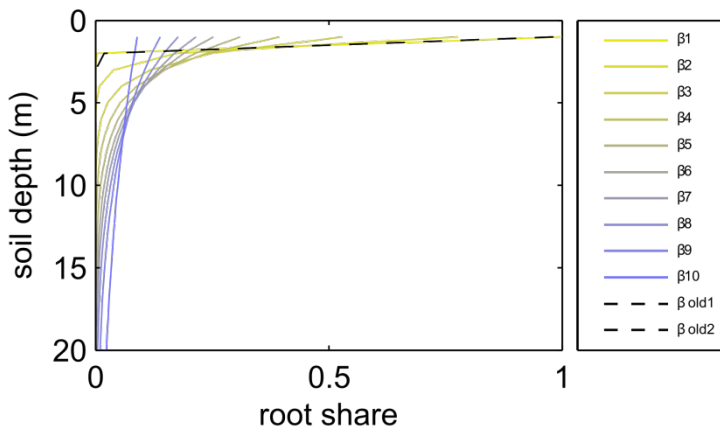
887 In LPJmL4.0 background mortality is modelled by a fractional reduction of PFT biomass, which depends on growth  
 888 efficiency (Schaphoff *et al.*, 2018a). This annual rate of mortality is limited by a constant maximum mortality rate of 3% of  
 889 tree individuals per year which is applied to all tree PFTs. In other words, the fastest total biomass loss of a tree PFT due to  
 890 low growth efficiency can happen within about 33 simulation years. In general, this maximum mortality rate can be regarded



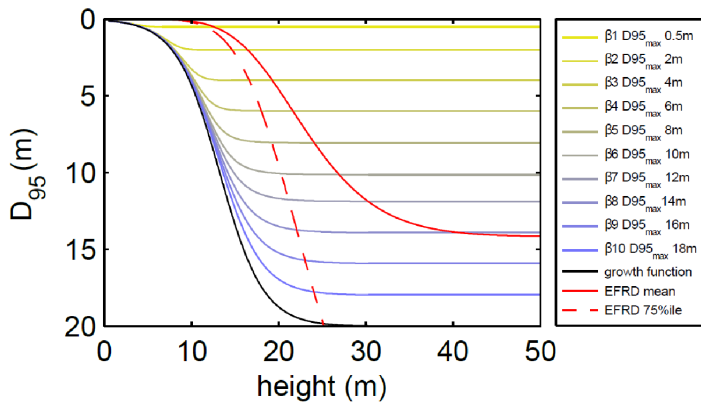
891 as a global tuning parameter of biomass accumulation as it caps the maximum biomass loss. Since many mechanisms  
 892 influencing tree mortality in the real world, e.g. hydraulic failure (Johnson et al., 2018), are not yet implemented in most  
 893 DGVMs including LPJmL4.0 (Allen et al., 2015), the parameterization of a background tree mortality remains a challenging  
 894 topic. Under the current model status of LPJmL4.0 maximum mortality rates are a necessary feature, while future model  
 895 development must overcome the concept of applying a maximum mortality rate by refining and implementing most  
 896 important mechanisms that influence tree mortality.

897 In LPJmL4.0-VR tree PFTs can access water in soil depths which were formerly inaccessible. This enhances the general  
 898 growth efficiencies of tree PFTs and consequently decreases their overall background mortality. Since global biomass  
 899 pattern simulated with LPJmL4.0 were already in acceptable range, the maximum background mortality in LPJmL4.0-VR  
 900 was calibrated and is now increased to 7% in order to counter-balance increased survival rates and therefore biomass  
 901 accumulation.

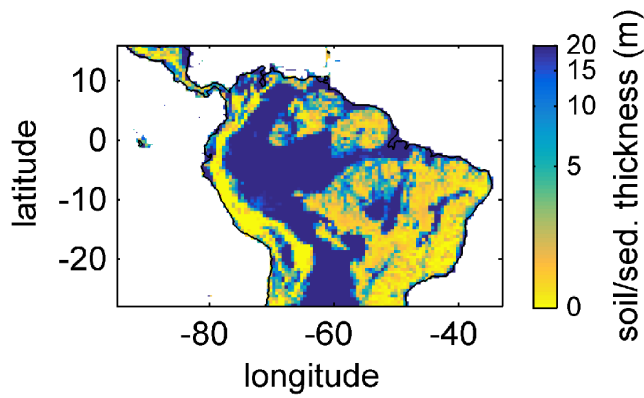
902 **1.8 Figures**



903  
 904 **Figure A1: Relative amount of fine roots in each soil layer for different  $\beta$ -values in LPJmL4.0 and LPJmL4.0-VR.** In the legend  
 905 “ $\beta$  old1-2” correspond to the  $\beta$ -values of the 2 tropical tree PFTs (deciduous and evergreen) simulated in LPJmL4.0. The  
 906 corresponding graphs lie on top of each other due to marginal differences in their  $\beta$ -values. “ $\beta$ 1-10” correspond to the 10  $\beta$ -values  
 907 used in LPJmL4.0-VR (Table A2) used to create the 10 sub-PFTs of the tropical evergreen and deciduous tree PFTs (Appendix A  
 908 Sect. 1.3). For LPJmL4.0-VR the fine root distribution at maximum rooting depth is shown. Please note, the first 3 soil layer (as  
 909 described in Appendix A Sect. 1.1) in this visualization are treated as 1 layer of 1 m thickness for reasons of visual clarity.



910  
 911 **Figure A2: Relation between tree height and rooting depth in LPJmL4.0-VR.** Black line: Implemented general growth function of  
 912 rooting depth (Eq. A5). Lines with colour scale from yellow to blue: Growth functions of rooting depth for each of the 10 sub-PFTs  
 913 (Sect. 2.2.3). Here temporal rooting depth is expressed as  $D_{95}$  and eventually reaches  $D_{95\_max}$  (Eq. A3). Red solid line: Mean  
 914 effective functional rooting depth over tree height (EFRD) adapted from Brum et al. (2019) using Eq. A5. Red dashed line:  
 915 Respective 75%ile EFRD over tree height adapted from Brum et al. (2019). Please also see Supplementary Video 1 for a  
 916 visualization of root growth and development of belowground carbon pools over time under [http://www.pik-](http://www.pik-potsdam.de/~borissa/LPJmL4_VR/Supplementary_Video_1.pptx)  
 917 [potsdam.de/~borissa/LPJmL4\\_VR/Supplementary\\_Video\\_1.pptx](http://www.pik-potsdam.de/~borissa/LPJmL4_VR/Supplementary_Video_1.pptx).



918  
919 **Figure A3: Soil/sediment thickness from (Pelletier et al., 2016) regridded to the 0.5° x 0.5° longitude-latitude grid of LPJmL4.0-VR**  
920 **and restricted to a maximum of 20 m. Colorbar in decadic logarithm.**  
921

922 **1.9 Tables**

923 **Table A1: Soil layer partitioning scheme used in LPJmL4.0-VR. The first meter of the soil column is split into 3 soil layers and**  
924 **after 1m of soil depth each following soil layer is assigned a thickness of 1 m as in LPJmL4.0. Whereas LPJmL4.0's last soil layer**  
925 **reaches 3 m, LPJmL4.0-VR's last soil layer reaches 20 m.**

Soil layer number	Soil layer boundary (m)	Soil layer thickness (m)
1	0.2	0.2
2	0.5	0.3
3	1	0.5
4	2	1
...	...	...
23	20	1

926 **Table A2:  $\beta$ -values assigned to the 10 sub-PFTs of each tropical PFT (evergreen and deciduous) in LPJmL4.0-VR and the**  
927 **corresponding maximum rooting depth reached by 95% of the roots ( $D_{95\_max}$ ).**

sub-PFT number	$\beta$ -value	$D_{95\_max}$ (m)
1	0.9418	0.5
2	0.9851	2
3	0.9925	4
4	0.995	6
5	0.9963	8
6	0.9971	10
7	0.9976	12
8	0.9981	14
9	0.9986	16
10	0.9993	18

928 **Table A3: Description of Fluxnet sites used for the evaluation of simulated ET.**

Site name	Short name	Country	LPJmL coordinate	
			latitude	longitude
Ecotone Bananal Island/BR-Ban	TOC_BAN	Brazil	-9.75	-50.25
Manaus-ZF2 K34/BR-Ma2	MAN_K34	Brazil	-2.75	-60.25
Santarem-Km67-Primary Forest/BR-Sa1	STM_K67	Brazil	-2.75	-54.75
Santarem-Km77-Pasture/BR-Sa2	STM_K77	Brazil	-3.25	-54.75
Santarem-Km83-Logged Forest/BR-Sa3	STM_K83	Brazil	-3.25	-54.75

Rond.- Rebio Jaru Ji Parana- Tower B/BR-Ji3	RON_RJA	Brazil	-10.25	-61.75
Guyaflux	GF_GUY	French Guiana	5.25	-52.75

929 **Appendix B**

930 **1 Results**

931 **1.1 Local evapotranspiration**

932 Differences of intra-annual rates of ET and NEE between the 3 LPJmL model versions are most pronounced at Fluxnet sites  
933 with high seasonality of rainfall (Fig. B6b, e, g and Fig. B7b, e, g). Here, variable tree rooting strategies (LPJmL4.0-VR)  
934 lead to a major improvement in reproducing measured Fluxnet NEE and ET, also expressed in reduced NME and increased  
935  $r^2$ -values (Table B1-B2). Whereas, constant tree rooting strategies (LPJmL4.0-VR-base and LPJmL4.0) simulate decreasing  
936 ET and increasing NEE during dry seasons at these sites, which is anticorrelated to Fluxnet measurements, variable tree  
937 rooting strategies (LPJmL4.0-VR) follow the intra-annual Fluxnet signals. Most pronounced improvements are found at  
938 STM K67 and STM K83, where the NME of ET and NEE drop below or close to 1, and where  $r^2$ -values considerably  
939 increase compared to the other 2 model versions (Table B1-B2). For STM K67, the  $r^2$  of NEE is higher under LPJmL4.0 and  
940 LPJmL4.0-VR-base, but this refers to a significant negative correlation.

941 At STM K77 (Fig. B6f) local circumstances show the influence of variable rooting strategies on ET in a different way. This  
942 former rainforest site was converted to pasture before Eddy covariance measurements began. This local land-use at STM  
943 K77 is not representative for the respective  $0.5^\circ$  grid cell, and thus all 3 LPJmL model versions simulate mainly natural  
944 vegetation instead of pasture. Therefore, the shallow rooting systems of LPJmL4.0 and LPJmL4.0-VR-base show a better  
945 match to ET measurements at STM K77. The site STM K83 (Fig. B6g) is a selectively logged primary forest site which  
946 shares the same model grid cell as STM K77 due to their geographical proximity. Again, here only simulations with variable  
947 tree rooting strategies (LPJmL4.0-VR) reproduce increased ET and decreased NEE during the dry season. At sites with  
948 weaker to no dry season (Fig. B6c, d, h) differences between model versions become less pronounced, as water availability is  
949 more stable throughout the year leading to less variable ET.

950 **1.2 Regional pattern of simulated above- and belowground biomass**

951 The simulated mean AGB pattern (2001-2010) of LPJmL4.0-VR (Fig. B10) shows that variable tree rooting strategies lead  
952 to a contiguous high biomass over the Amazon region. Especially towards the borders of the South-Eastern Amazon region  
953 in the climatological clusters EQ E and SAMz, AGB values appear rather homogenous in contrast to constant shallow tree  
954 rooting strategies simulated in the other 2 model versions (Fig. B10d-e). In connection with the significantly improved  
955 underlying vegetation composition (Fig. 4e-f) it is clear that LPJmL4.0-VR is the only model version capable of simulating  
956 high AGB evergreen rainforests across the climatic gradient of the Amazon region (Fig. B1-B2). This pattern is also found  
957 by one satellite derived AGB product chosen for evaluation of our model results (Saatchi *et al.*, 2011; Fig B10b) which  
958 yields a corresponding NME close to 0 (Table B6). However, compared to this product low NME values are found for all  
959 model versions. Surprisingly, in comparison to the other AGB validation product (Avitabile *et al.*, 2016a; Fig. B9a)  
960 LPJmL4.0-VR-base yields a smaller NME than LPJmL4.0-VR. Considering the significantly less accurate underlying  
961 vegetation composition of LPJmL4.0-VR-base as well as LPJmL4.0 (Fig. 4) we regard such comparisons as critical in this  
962 context.

963 Comparisons of AGB pattern between all model versions of this study and different biomass products are difficult, since  
964 only LPJmL4.0-VR shows a reasonable geographical distribution of underlying PFTs across the study area (Fig. 4, Table  
965 B4). Therefore, differences in biomass are not solely the consequence of different productivities directly related to diversity

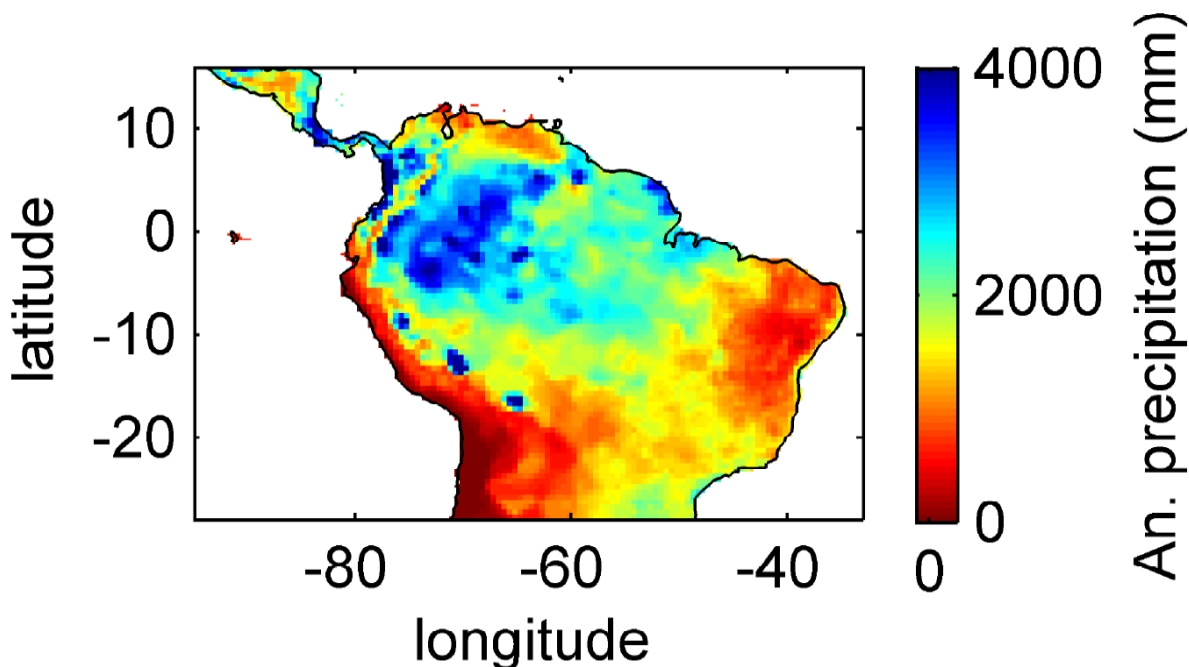
966 in tree rooting strategies, but also the consequence of simulated PFT dominance, i.e. rather an indirect effect of diversity in  
967 tree rooting strategies. Concentrating on LPJmL4.0-VR only, the model matches substantially better with the gridded  
968 biomass product of Saatchi et al. (2011; Table B5), since this product shows generally higher biomass values across the  
969 Amazon region which are more similar to LPJmL4.0-VR. Therefore, the higher NME found in the comparison to the  
970 biomass product of Avitabile et al. (2016) is mainly caused by divergence of mean biomass values of the evergreen PFT  
971 across the whole study area rather than pattern divergence. Thus, we argue lowering overall biomass values in LPJmL4.0-  
972 VR would improve its match with Avitabile et al. (2016) which is a matter of adjusting overall maximum tree mortality rates  
973 (Appendix A Sect. 1.7).

974 Simulating diverse tree rooting strategies in connection with investment into coarse root structures in LPJmL4.0-VR allows  
975 analysing carbon investment into the newly implemented root carbon pools (Appendix A Sect. 1.4 & Sect. 2.2). As expected,  
976 belowground biomass (BGB; Fig. B9) follows the simulated pattern  $\overline{D_{95}}$  (Fig. 2). Highest BGB is found at maximum values  
977 of  $\overline{D_{95}}$  and vice versa.

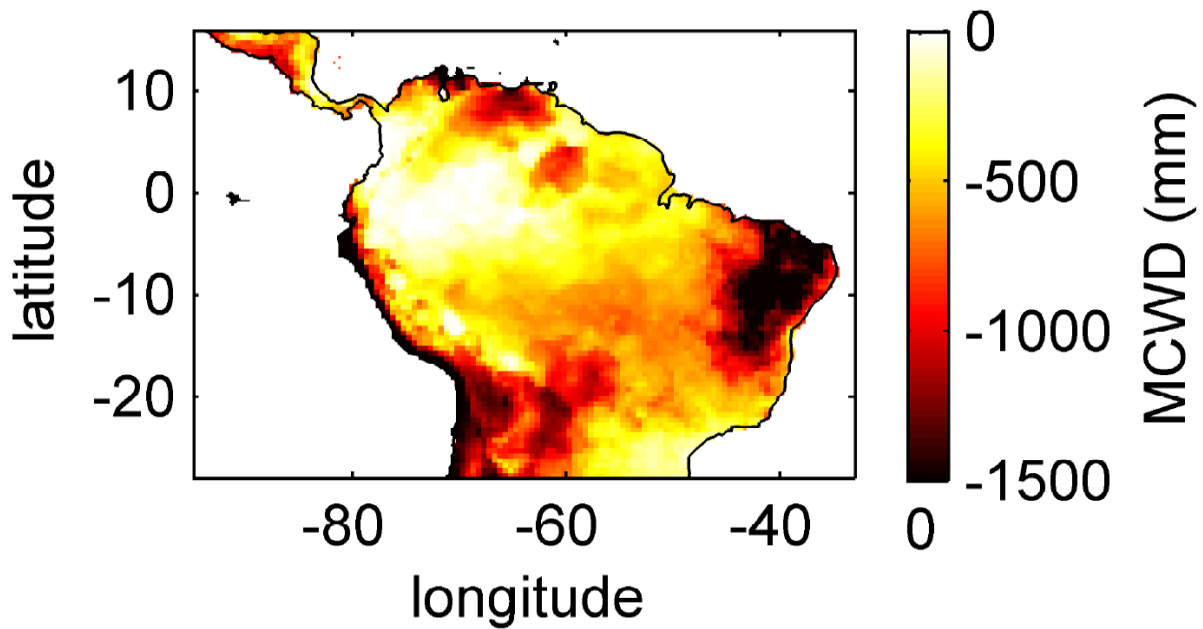
978 It is important to note that LPJmL4.0-VR appears to underestimate BGB compared to empirical findings in the Amazon  
979 region. While LPJmL4.0-VR shows BGB making up a range of 3.6-16.2% of total biomass across the Amazon region,  
980 different site specific empirical studies found mean values at the upper end or significantly exceeding this range (Fearnside,  
981 2016). The most plausible explanation for underestimating BGB is that LPJmL4.0-VR does not account for root structures  
982 needed for tree statics. Acknowledging tree statics would increase below ground carbon investment and therefore BGB.  
983 Nevertheless, below-ground carbon investment for tree statics would apply for all sub-PFTs simultaneously and would  
984 therefore most likely not significantly change competition dynamics and resulting distributions of tree rooting strategies  
985 found in this study.

### 986 1.3 Figures

987

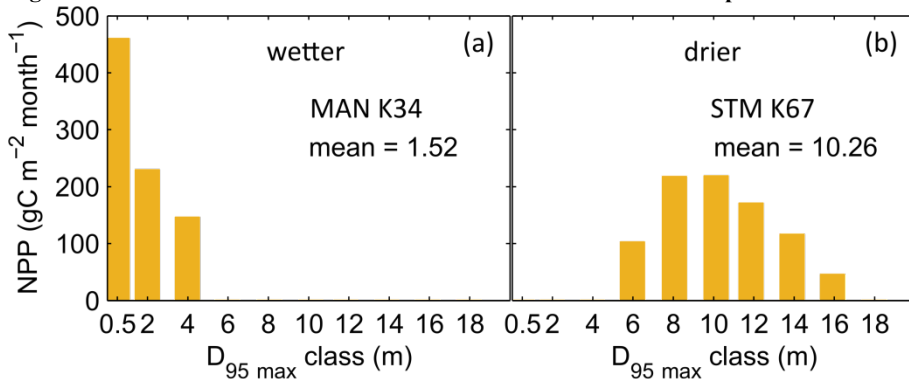


988  
989 **Figure B1: Mean annual precipitation for 2001-2010 under CRU climate input.**



990  
991

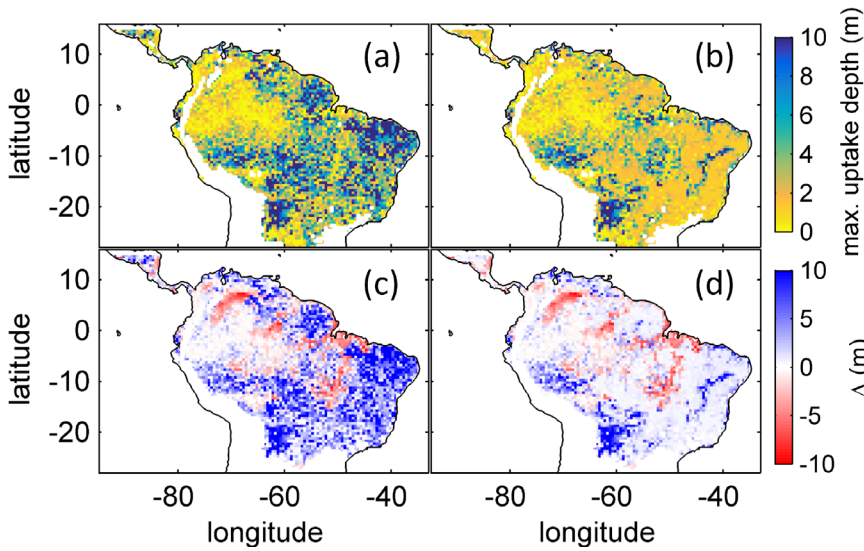
Figure B2: Mean annual MCWD for 2001-2010 under CRU climate input.



992

993  
994  
995  
996  
997  
998  
999  
1000  
1001  
1002  
1003  
1004

Figure B3: Distributions of simulated mean monthly NPP for each  $D_{95\_max}$ -class for 2001-2010 under CRU climate input at two FluxNet sites. a) Site MAN K34 near the city of Manaus. b) Site STM K67 near the city of Santarem. For more site information see Table A3 and Fig. B6a. At the Fluxnet site MAN K34 (a), which exhibits a mean annual precipitation (MAP) of 2609 mm and a mean MCWD of -222 mm under CRU climate input (2001-2010), the sub-PFT with a maximum rooting depth ( $D_{95\_max}$ ) of 0.5 m contributes most to overall NPP and the whole distribution of NPP weighted  $D_{95\_max}$  classes shows a mean of 1.52 m. At the Fluxnet site STM K67 (b), which exhibits a lower MAP of 2144 mm and a stronger dry season reflected in a mean MCWD of -465 mm, the NPP weighted distribution of  $D_{95\_max}$  shows a peak at 10 m and a corresponding mean of 10.26 m. Since both sites have a soil depth of 20 m (according to the soil depth input; Sect. 2.3.2, Fig. A3) differences in rooting strategy compositions must emerge from the climatic differences of those sites. It is important to note that  $D_{95\_max}$  values (i.e. the bins on the x-axes) do not necessarily reflect the true achieved rooting depth of each sub-PFT, but their maximum value. For reasons of visual clarity for this figure we kept the bins of the x-axes as chosen in Table A2.



1005

1006

1007

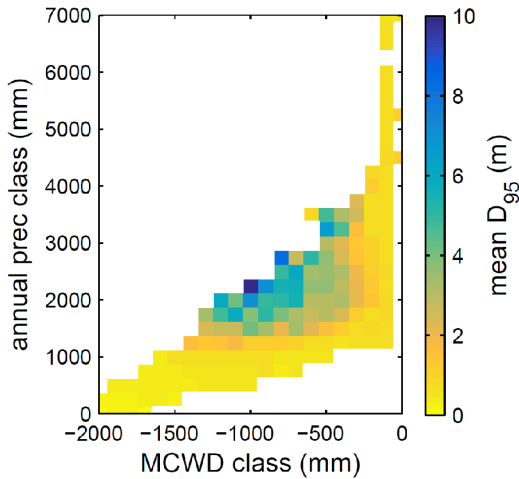
1008

1009

1010

1011

**Figure B4: Comparison of simulated  $\overline{D_{95}}$  to product of maximum tree root water uptake depth (MDRU). a) Original (Fan et al., 2017) MDRU regridded to  $0.5^\circ \times 0.5^\circ$  resolution of LPJmL4.0-VR. b) Same as a) but adjusted to soil depth input used in this study (see 2.3.2), in cases where values of (Fan et al., 2017) exceeded this soil depth. The color scale maximum for a) and b) is set to 10 m. c) Difference between a) and  $\overline{D_{95}}$  simulated with LPJmL4.0-VR under CRU climate forcing (Fig. 2a). d) Difference between b) and  $\overline{D_{95}}$  simulated with LPJmL4.0-VR under CRU climate forcing (Fig. 2a). Red/blue colors denote higher/lower rooting depths in LPJmL4.0-VR.**



1012

1013

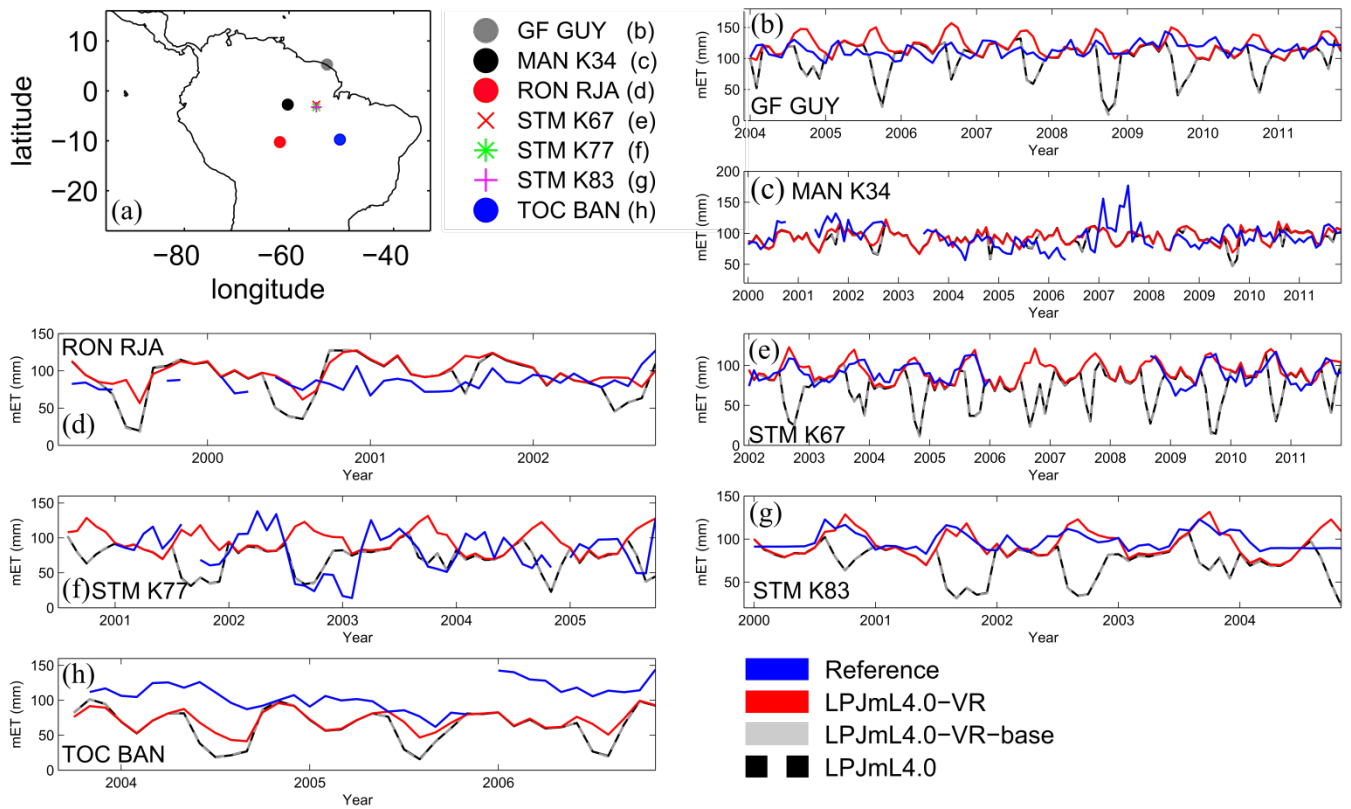
1014

1015

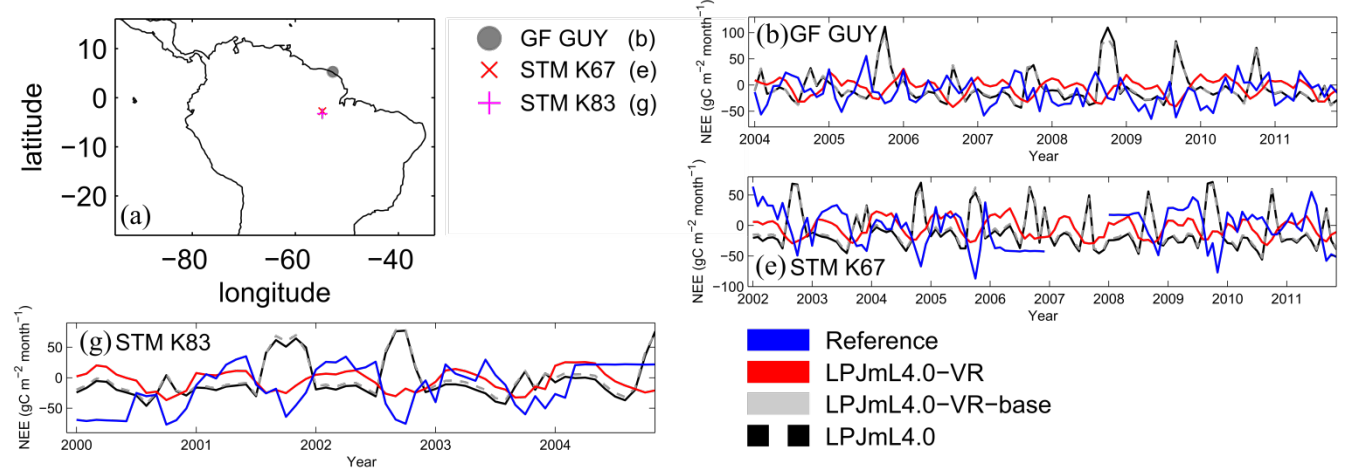
1016

1017

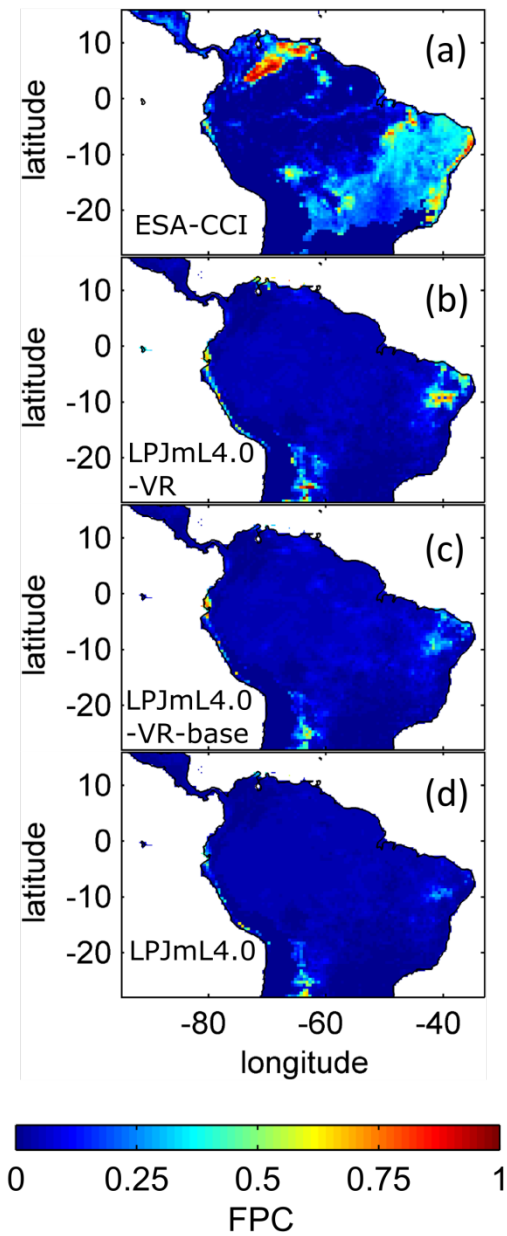
**Figure B5: Mean rooting depth depicted as mean  $\overline{D_{95}}$  over classes of MCWD and annual precipitation sums. Class step size for precipitation was set to 250 mm and class size for MCWD was set to 50 mm. Regions with high amounts of annual rainfall and lower seasonality exclusively favour shallow rooted forests (low  $\overline{D_{95}}$ ).  $\overline{D_{95}}$  increases with decreasing MCWD (increasing seasonal drought stress) and decreasing sums of annual precipitation. Below 1200 mm of annual rainfall or -1100 mm of MCWD  $\overline{D_{95}}$  sharply decreases again. Note this figure does not consider soil depth. The color scale maximum is set to 10 m.**



1018  
1019  
1020  
1021  
**Figure B6:** Comparisons of monthly ET between different Fluxnet sites (“Reference”; see also Sect. 2.5.1) and respective simulation output of the different LPJmL model versions used in this study forced with CRU climate. a) Geographical location of different Fluxnet sites (see also Table A3). For statistical measures of the individual comparison see Table B1.

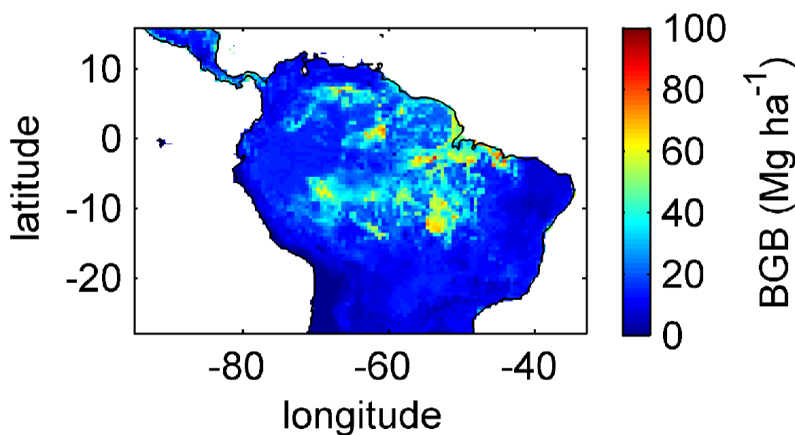


1022  
1023  
1024  
1025  
1026  
1027  
**Figure B7:** Comparisons of monthly NEE between different Fluxnet sites (“Reference”; see also Sect. 2.5.1) and respective simulation output of the different LPJmL model versions used in this study forced with CRU climate. a) Geographical location of different Fluxnet sites (see also Table A3). For statistical measures of the individual comparison see Table B2. Note due to data scarcity only 3 Fluxnet sites are shown. Plots of all sites are shown in Fig. B12. We kept panel labelling as in Fig. B6 to ensure easy comparability.



1028  
1029  
1030  
1031  
1032

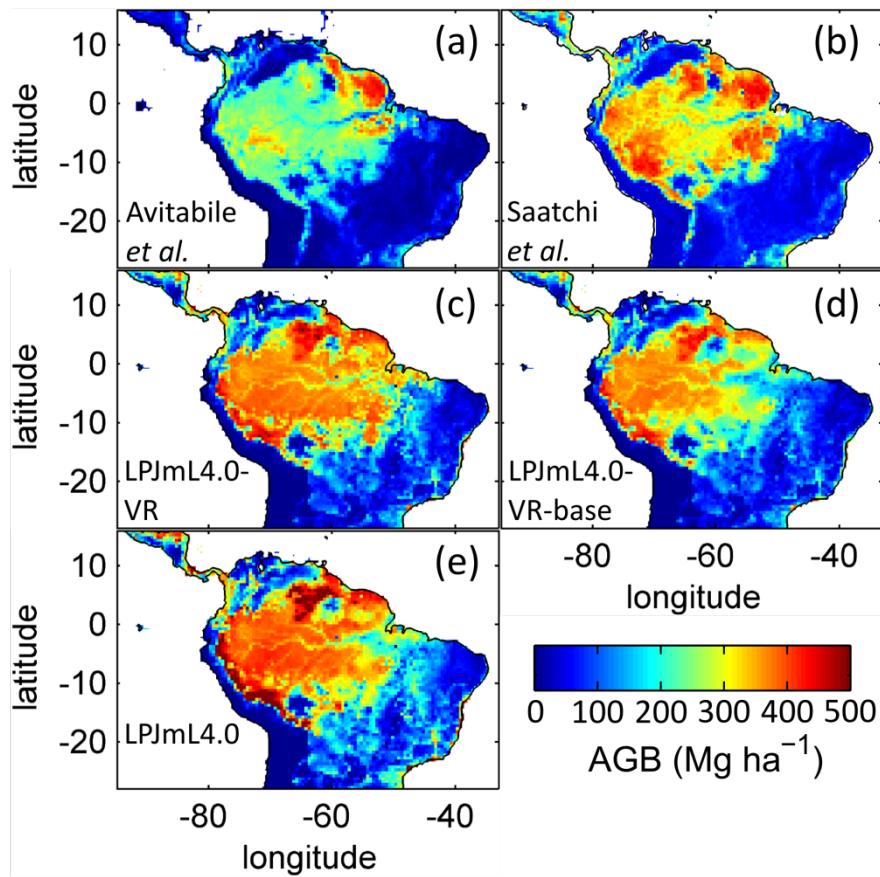
Figure B8: Foliage projected cover (FPC) of the tropical herbaceous PFT over the study region. a) Satellite-derived vegetation composition from ESA Land cover CCI V2.0.7 (Li et al., 2018) reclassified to the PFTs of LPJmL as in (Forkel et al., 2014). b) LPJmL4.0-VR. c) LPJmL4.0-VR-base. d) LPJmL4.0. All LPJmL model versions were forced with CRU climate input. The shown FPC for all models refers to 2001-2010.



1033  
1034  
1035

Fig. B9: Mean sum (2001-2010) of belowground biomass (BGB; sum of tree coarse and fine roots) of evergreen and deciduous tree PFTs simulated with LPJmL4.0-VR under CRU climate forcing.





1036

1037

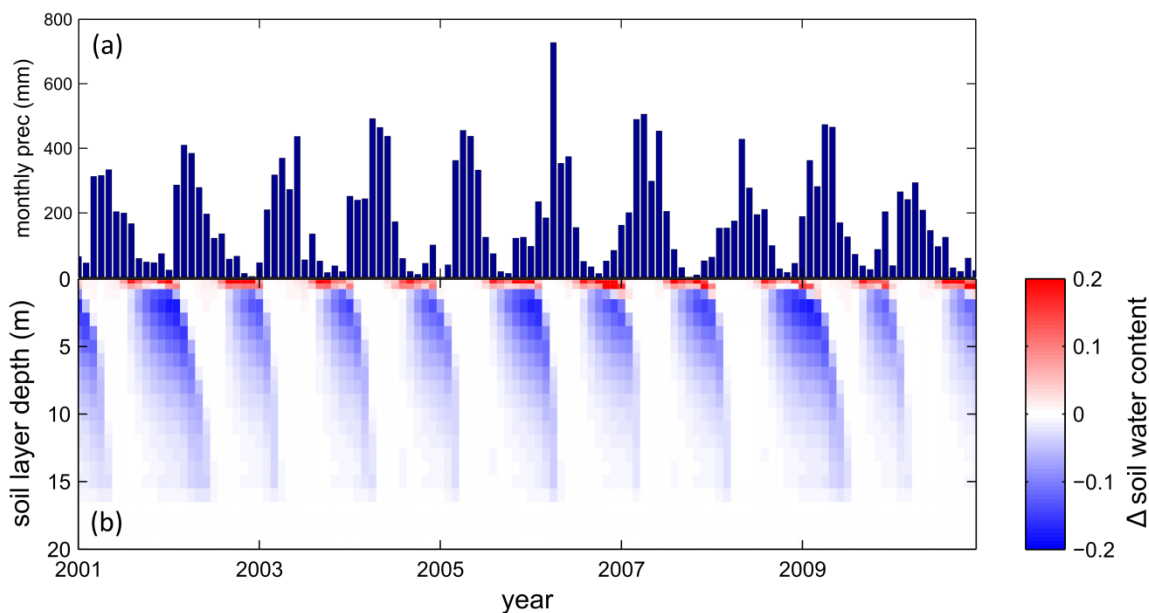
1038

1039

1040

1041

**Fig. B10:** Comparison of simulated AGB and satellite derived AGB validation products regridded to the spatial resolution of LPJmL models. a) Biomass validation product from Avitabile et al. (2016b). b) AGB validation product from Saatchi et al., (2011). c-e) Mean AGB simulated for the time span 2001-2010 with c) LPJmL4.0-VR. d) LPJmL4.0-VR-base and e) LPJmL4.0. For statistical measures of individual comparisons between model versions (c-e) and satellite derived AGB evaluation products (a-b) see Table A7.



1042

1043

1044

1045

1046

1047

**Figure B11:** Difference in soil water reaction to seasonal precipitation between LPJmL4.0-VR-base and LPJmL4.0-VR at Fluxnet site STM KM67 a) Mean monthly precipitation input from CRU for 2001-2010. b) Difference in monthly relative soil water content between LPJmL4.0-VR-base and LPJmL4.0-VR forced with CRU climate for 2001-2010. The underlying model output variable “soil water content” of each model version is a number between 0 and 1 depicting the relative water saturation of the soil. Blue colors denote lower soil water content in LPJmL4.0-VR and red colors a lower soil water content in LPJmL4.0-VR-base.

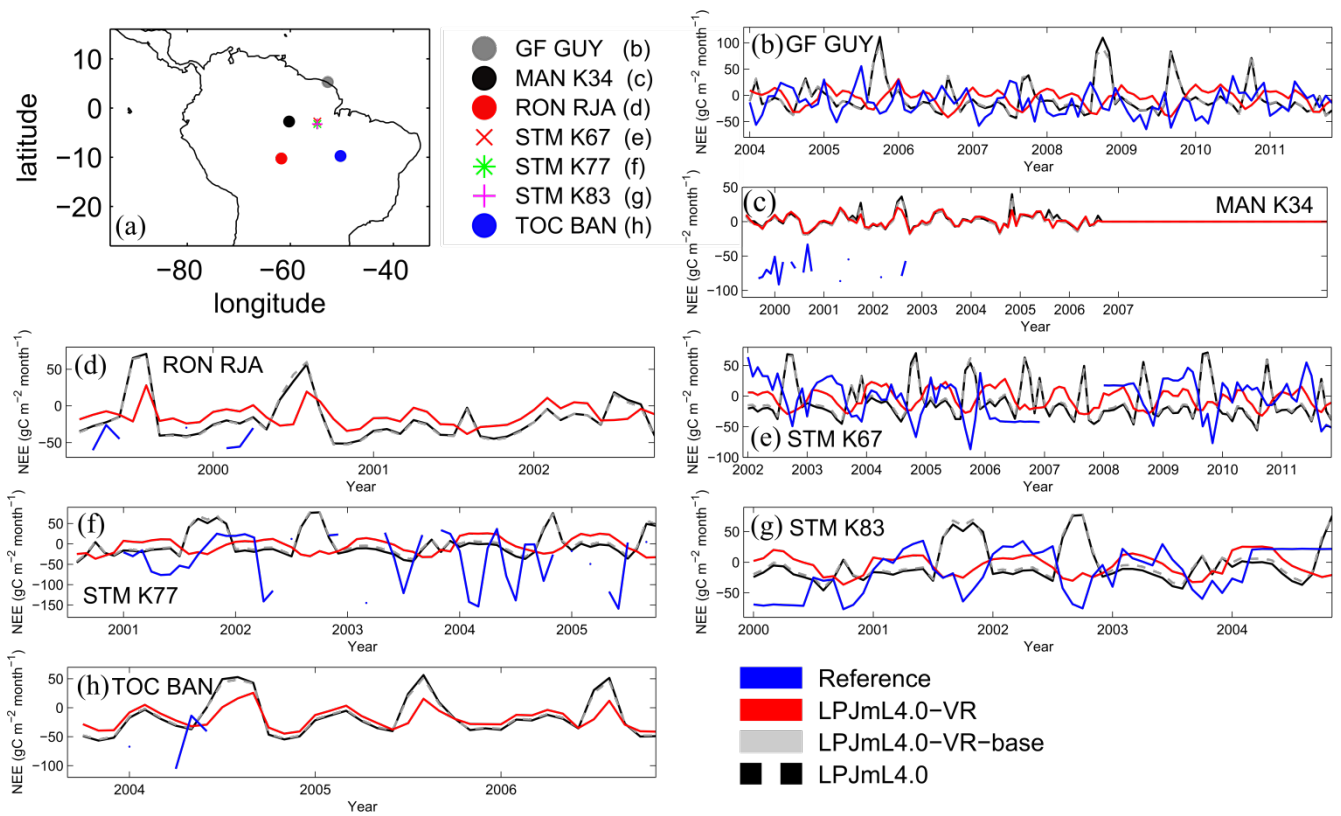


**Fig. B12:** Comparisons of monthly NEE between different Fluxnet sites (“Reference”; see also Sect. 2.5.1) and respective simulation output of the different LPJmL model versions used in this study forced with CRU climate. a) Geographical location of different Fluxnet sites (see also Table A2).

#### 1.4 Tables

**Table B1:** Normalized mean error (NME), coefficient of determination ( $r^2$ ) and p-value of F-statistic piecewise calculated for simulated ET of the different LPJmL model versions used in this study forced with CRU climate input and Fluxnet data of ET at 7 Fluxnet sites (in accordance with Fig. B6).

Statistic	Model	TOC BAN	MAN K34	STM K67	STM K77	STM K83	RON RJA	GF GUY
NME	LPJmL4.0-VR	2.41	1.11	0.75	1.38	1.10	2.28	1.57
	LPJmL4.0-VR-base	2.92	1.22	2.29	0.98	2.74	2.73	2.38
	LPJmL4.0	2.93	1.23	2.27	0.98	2.74	2.70	2.36
$r^2$	LPJmL4.0-VR	0.09	0.03	0.53	0.17	0.43	0.01	0.08
	LPJmL4.0-VR-base	0.10	0.00	0.33	0.14	0.03	0.01	0.01
	LPJmL4.0	0.09	0.00	0.33	0.14	0.03	0.01	0.01
p-value	LPJmL4.0-VR	0.075	0.041	< 0.001	0.002	< 0.001	0.575	0.005
	LPJmL4.0-VR-base	0.067	0.585	< 0.001	0.005	0.221	0.517	0.277
	LPJmL4.0	0.068	0.672	< 0.001	0.005	0.221	0.514	0.274

**Table B2:** Normalized mean error (NME), coefficient of determination ( $r^2$ ) and p-value of F-statistic piecewise calculated for simulated NEE of the different LPJmL model versions used in this study forced with CRU climate input and Fluxnet data of NEE at 3 Fluxnet sites (in accordance with Fig. B7).

Statistic	Model	STM K67	STM K83	GF GUY
NME	LPJmL4.0-VR	0.90	0.84	1.30
	LPJmL4.0-VR-base	1.62	1.36	1.52
	LPJmL4.0	1.68	1.39	1.52
$r^2$	LPJmL4.0-VR	0.16	0.14	0.00
	LPJmL4.0-VR-base	0.32	0.06	0.03
	LPJmL4.0	0.33	0.07	0.03
p-value	LPJmL4.0-VR	< 0.001	0.003	0.515
	LPJmL4.0-VR-base	< 0.001	0.055	0.046
	LPJmL4.0	< 0.001	0.047	0.059

1060

1061  
1062  
1063  
1064  
1065

**Table B3: Normalized mean error (NME), coefficient of determination ( $r^2$ ) and p-value of F-statistic piecewise calculated for the simulated ET of the different LPJmL model versions used in this study and continental scale gridded ET products within 5 regional climatological clusters. With respect to Fig. 3 comparisons are based on the monthly mean of corridors shown, i.e. 1) the monthly mean of all outputs produced by one LPJmL model version but forced with different climate inputs and 2) the monthly mean of all continental scale gridded ET data products.**

Statistic	Model	NSA	EQ W	EQ E	SAmz	SAMS
NME	LPJmL4.0-VR	0.08	0.26	0.62	0.20	0.06
	LPJmL4.0-VR-base	0.37	0.42	1.95	0.58	0.13
	LPJmL4.0	0.34	0.26	1.92	0.58	0.11
$r^2$	LPJmL4.0-VR	0.98	0.94	0.91	0.98	1.00
	LPJmL4.0-VR-base	0.94	0.96	0.20	0.91	0.99
	LPJmL4.0	0.93	0.96	0.21	0.90	0.99
p-value	LPJmL4.0-VR	< 0.001	< 0.001	< 0.001	< 0.001	< 0.001
	LPJmL4.0-VR-base	< 0.001	< 0.001	0.143	< 0.001	< 0.001
	LPJmL4.0	< 0.001	< 0.001	0.135	< 0.001	< 0.001

1066  
1067  
1068  
1069

**Table B4: Normalized mean error (NME) of FPC comparison piecewise calculated between 1) the satellite-derived vegetation composition from ESA Land cover CCI V2.0.7 (Li et al., 2018) reclassified to the PFTs of LPJmL as in Forkel et al. (2014) and 2) all LPJmL model versions used in this study forced with CRU climate data (in accordance with Fig. 4).**

Statistic	Model	FPC Evergreen	FPC Deciduous
NME	LPJmL4.0-VR	0.31	1.01
	LPJmL4.0-VR-base	0.38	1.5
	LPJmL4.0	0.47	1.76

1070

1071  
1072  
1073

**Table B5: Normalized mean error (NME) of AGB comparison piecewise calculated between 1) the satellite-derived AGB validation products and 2) all LPJmL model versions used in this study forced with CRU climate data (in accordance with Fig. B10).**

Statistic	Model	Avitabile <i>et al.</i>	Saatchi <i>et al.</i>
NME	LPJmL4.0-VR	0.78	0.12
	LPJmL4.0-VR-base	0.69	0.11
	LPJmL4.0	1.09	0.14

1074